



HAL
open science

Spent fuel transportation cask under accidental fire conditions: Numerical analysis of gas transport phenomena affecting heat transfer in shielding materials

Matthieu Zinet, Roula Ghazal, Hervé Issard, Olivier Bardon

► To cite this version:

Matthieu Zinet, Roula Ghazal, Hervé Issard, Olivier Bardon. Spent fuel transportation cask under accidental fire conditions: Numerical analysis of gas transport phenomena affecting heat transfer in shielding materials. *Progress in Nuclear Energy*, 2019, 117, pp.103045. 10.1016/j.pnucene.2019.103045 . hal-02432891

HAL Id: hal-02432891

<https://hal.science/hal-02432891>

Submitted on 22 Oct 2021

HAL is a multi-disciplinary open access archive for the deposit and dissemination of scientific research documents, whether they are published or not. The documents may come from teaching and research institutions in France or abroad, or from public or private research centers.

L'archive ouverte pluridisciplinaire **HAL**, est destinée au dépôt et à la diffusion de documents scientifiques de niveau recherche, publiés ou non, émanant des établissements d'enseignement et de recherche français ou étrangers, des laboratoires publics ou privés.



Distributed under a Creative Commons Attribution - NonCommercial 4.0 International License

Spent Fuel Transportation Cask under Accidental Fire Conditions: Numerical Analysis of Gas Transport Phenomena Affecting Heat Transfer in Shielding Materials

Matthieu Zinet^{a*}, Roula Ghazal^b, Hervé Issard^b, Olivier Bardon^b

^a Univ Lyon, Université Lyon 1, CNRS UMR 5223, Ingénierie des Matériaux Polymères, F-69622 Villeurbanne, France

^b ORANO TN International, 1 rue des Hérons, 78180 Montigny-le-Bretonneux, France

*Corresponding author. Email: matthieu.zinet@univ-lyon1.fr

Abstract

In the nuclear industry, spent fuel is usually conveyed to the reprocessing or long term storage facilities in dedicated containers: the transportation casks. These structures are designed to meet rigorous standards intended to prevent any failure under both normal transport and severe accidental conditions. The design process includes thermal analyses in order to predict the temperature response of the cask to a 30 minutes engulfing fire at 800°C. Materials presenting endothermic decomposition reactions are often used as thermal and radiologic protection in the cask walls. This paper focuses on numerically investigating the secondary effects induced by the vapor transfer phenomena specific to these endothermic shielding materials, using finite element modeling of heat transfer within the wall of a typical cask. Mechanisms such as vaporization, diffusion and recondensation of the water content, resulting in a transfer of latent heat within the medium, are taken into account in the model. Three materials are considered: polyester resin compound, plaster and phenolic foam. The predictions of this detailed model are compared to those of a model assuming only conduction heat transfer. It is shown that gas transport phenomena have a significant effect on the heating kinetics. Finally, the influence of model parameters such as the material porosity and the condensation coefficient is discussed.

Keywords: spent fuel transport, heat transfer analysis, thermal decomposition reactions, finite element modeling

1 Introduction

During the back end of the nuclear fuel cycle, a transportation stage is required to move spent nuclear fuel (SNF) from interim storage located on the sites of the utilization facilities (reactor of nuclear power plant or research facilities) to reprocessing and / or long-term storage facilities. The transport is usually achieved by loading the radioactive materials into a specially designed container of large dimensions, the transportation cask. The shipment may involve transport by a combination of different modes: road, rail, sea and even air. In order to ensure, at any moment, the protection of workers, the public and the environment, the packaging system must fulfill several functions: confinement of the nuclear materials, mechanical protection, thermal protection, radiologic shielding. It must also allow convenient loading, drying, tightening and handling procedures to limit the operation times and costs.

Basically, the body of a transportation cask has the shape of a hollow cylinder **(Figure 1)**, whose wall consists of at least three concentric layers: the outer steel shell in contact with the exterior environment, a thick shielding material layer ensuring the thermal protection and neutron absorption functions, and the inner steel shell enclosing the cavity in which the hazardous materials are stored. The latter can be either vitrified wastes sealed into steel canisters or spent fuel rods encapsulated in a metal cladding and arranged according to a grid layout into a basket holding the fuel assemblies. A tight lid closes the cavity. Both ends of the cask are fitted with shock absorbers for mechanical integrity in case of severe impact.

In order to ensure compliance with international safety requirements set by the International Atomic Energy Agency (IAEA, 2012), the packaging specifications are expected to meet rigorous standards intended to guarantee its integrity under both normal transport and severe accidental conditions. For this purpose, the cask prototype is subjected to standardized tests mimicking the conditions encountered in the event of a potential accident: impact, perforation, fire, immersion. Throughout the design, sizing and accreditation phases, various numerical simulations are carried out in order to predict and assess the behavior of the packaging during these tests. More specifically, thermal analyses

are conducted in order to simulate the exposition of the cask to an accidental engulfing fire characterized by a radiative source at 800°C emitting for a time span of 30 minutes and to evaluate the maximum temperatures reached inside the cask as well as the heating kinetics. Such numerical simulations are usually performed on the basis of a 2D model of a transversal section (Bajwa, 2002) or a 3D model of the whole packaging (Bajwa et al., 2004),(Lo Frano et al., 2011),(Lo Frano et al., 2014),(Pugliese et al., 2010), with radiation boundary conditions to represent the heat flux exchanged between the fire and the cask, heat conduction in the solid parts of the system, in some cases partial melting of the content (Sanyal et al., 2011), or convection (natural or/and forced if a ventilation system is involved, mainly for storage casks (Alyokhina, 2018)) in the air volumes. Equivalence methods can be used to represent the complex multilayer structure of the cask wall and contents (including air gaps) (Xu et al., 2013),(Alyokhina and Kostikov, 2014). The model is then solved using the finite element method (FEM) or the finite volume method (FVM). In addition, some researchers were able to compare their simulation predictions to experimental thermal measurements carried out on the actual cask (Saliba et al., 2014) or a reduced scale mock-up (Lo Frano et al., 2018).

This approach has been widely used at the industrial level and has proven to be quite satisfying. However questions begin to arise from safety authorities concerning the validity of the heat transfer model in the case of shielding materials likely to undergo significant transformations when their temperature increases. This is in particular the case of the so-called “endothermic” materials. These material usually exhibit good mechanical, thermal insulation and fire-retardant properties. When submitted to the accidental fire test, the carbonized zone remains quite thin compared to the total thickness of the shielding, which ensures integrity of the package content. However, these materials contain water under various forms (free water, chemically bound water) or undergo thermally activated chemical reactions that produce water. As the material is heated, water vapor is released and a certain amount of calorific energy is absorbed in the form of latent heat. In the case of free water, the absorbed energy corresponds solely to latent heat of vaporization, whereas in the case of dehydration or decomposition reactions, the absorbed energy corresponds to the enthalpy of the

reaction. These endothermic transformations absorb a significant part of the heat transferred by the fire, thus limiting the temperature increase inside the cask. Moreover, the water vapor released can diffuse in the porous structure of the material to some extent and a fraction of this vapor can recondensate in colder areas of the material, which results in a return of latent heat to the latter. Hence, overall heat transfer is potentially affected by this gas transport mechanism: considering only conduction heat transfer in the endothermic material may not be sufficient. A variety of endothermic materials can be used for cask wall shielding: organic materials such as polymer resin compounds and polymer foams, inorganic materials such as plaster, or organic-inorganic hybrid materials such as “compounds” (e.g. a composite mix of plaster, high-density polyethylene and colemanite) (Droste, 2007; Gendreau et al., 2012; Issard, 2015)

The aim of this paper is to present and discuss a detailed strategy for investigating the secondary effects induced by the vapor transfer phenomena specific to these endothermic shielding materials, using finite element modeling of heat transfer within the wall of a typical cask. Mechanisms such as vaporization, diffusion and recondensation of the water content, resulting in a transfer of latent heat within the medium, are taken into account in the model. The modeling approach will be developed, tested and analyzed on a simplified geometry consisting of a two-dimensional transversal section of the wall. The numerical simulations will be performed using the finite element method. Three endothermic materials will be considered to assess the behavior of the model: polyester resin compound, plaster and high density phenolic foam. These materials are currently used in the design of transportation casks for their interesting mechanical and thermal properties, yet they belong to distinct physico-chemical nature and display different microstructures, which can lead to different thermal behavior, which is worth investigating. The temperature predictions of this comprehensive approach will be compared to those of a simpler approach taking into account only conduction heat transfer. In addition, a detailed analysis of the simulated mass transfer phenomena will be presented in order to highlight and explain the dependence of the heat transfer phenomena on the material nature and reaction characteristics (temperature range, enthalpy, amount of water released). Finally,

the influence of model parameters such as the material porosity and the condensation coefficient (difficult to quantify accurately) will be assessed.

2 Geometry and Materials Data

2.1 Modeled geometry

A typical cask wall consists of two stainless steel cylindrical shells (outer shell and inner shell) separated by the so-called endothermic shielding material (resin compound, plaster, polymeric foam, etc.). In packages intended to receive thermally active content, radial metallic (copper-based) fins can be intercalated at regular angular positions in order to increase heat transfer between the inner shell and the outer shell, which helps preventing buildup of residual heat in the cavity. During manufacturing, the empty spaces between radial fins and both shells form closed compartments in which the shielding material is poured before solidifying. Due to this process, the blocks of shielding material undergo a slight volumetric shrinkage resulting in a clearance (or gap) between the fin surfaces and the shielding material blocks surfaces. The metallic fins also participate in the overall mechanical strength of the wall. A cross-sectional view of the cask wall is shown in **Figure 2**. This geometry has been chosen as it is representative of most packaging currently designed. Thermal conductors have been taken into account in order to evidence and evaluate possible temperature inhomogeneity on the inner shell. The outer diameter of typical casks such as the one studied in this paper is about 500 mm. Since the axial length of the cylindrical wall is about 10 times larger than its diameter, the heat transfer analysis can be performed on a 2D model of the cask wall cross-section with reasonable accuracy. Moreover, such a cross-section contains radial symmetry planes, allowing to reduce the size of the computational domain to an angular sector equal to π/n_{fin} , where n_{fin} is the number of metallic fins.

2.2 Polyester resin compound

Polymers used as shielding materials in transportation casks are usually based on thermoset unsaturated polyester or vinylester resins (Issard, 2015). In addition to their role of self-extinguishing thermal and fire protection, these compounds also ensure radiation protection of the direct

environment of the cask by neutron shielding. For this purpose, they also contain additional fillers such as hydrogenated inorganic compounds to slow down neutrons (alumina hydrate in particular) and inorganic boron compounds to ensure uptake of the neutrons (zinc borate in particular). The shielding polyester resin compound belongs to this class of polymer compounds and is currently used in several commercialized transportation casks (Issard, 2009). When subjected to a temperature rise, the polyester resin compound exhibits several thermal decomposition phenomena (Mouritz and Gibson, 2007): vaporization of water in saturation in the alumina around 100°C, modification of alumina structure around 300°C and other subsequent degradation reactions. These reactions are accompanied by endothermic peaks (latent heat absorption) and releasing of gases such as water vapor. In particular, water vapor is likely to diffuse in the porous structure of the material and to recondensate in neighboring areas if the temperature remains below a condensation threshold around 100°C (due to the presence of depressurization devices in the cask wall), which leads to a return of energy to the material in the form of latent heat.

2.2.1 Degradation reactions

Schematically, the PE resin compound undergoes three successive decomposition reactions. The latent heat amounts as well as the temperature ranges associated with each reaction are known. However, in order to model the gas transfer, it is necessary to estimate the amount of water vapor released. The total water content of the resin compound before degradation is 22.5%, of which 21.5% in alumina hydrate and 1% in zinc borate, thus corresponding to 225 g of water per kg of resin compound (IPSN/AREVA internal report, 2001). During the first decomposition reaction R1, the water in saturation in alumina is vaporized. This reaction takes place in the temperature range 110°C - 140°C, which corresponds to a duration of about 5 minutes if an average heating kinetics of 6K/min is considered.

Assuming that the latent heat of this transformation ($\Delta H_{R1} = 10^5 \text{ J.kg}^{-1}$) corresponds entirely to the vaporization of the water, the latent heat of vaporization of the water being $\Delta H_{vap} = 2.257 \times 10^6 \text{ J.kg}^{-1}$, it can be deduced that a maximum mass of water corresponding to $\Delta H_{R1}/\Delta H_{vap}$ can be released during reaction R1, *i.e.* 45 g H₂O per kg of resin compound. It is assumed that the remaining water mass (180

g per kg of resin compound) is distributed in proportion to the total enthalpies of the subsequent reactions:

- reaction R2 (250°C – 270°C, about 3 min 30s at 6K/min): 137 g H₂O per kg of resin compound ($\Delta H_{R2} = 1.6 \times 10^6$ J/kg) ;
- reaction R3 (300°C – 380°C, about 13 min 30s at 6K/min): 43 g H₂O per kg of resin compound ($\Delta H_{R3} = 5 \times 10^5$ J/kg).

Moreover, it is assumed that these amounts of water are released in proportion to the advancement of the reactions. One should note that this approach may lead to overestimating the amount of water actually released, but it is conservative. The advancement degree of each reaction g_i ($i = 1, 2, 3$) is supposed to follow a sigmoidal evolution between 0 and 1, delimited by the reaction start and end temperatures mentioned above, which can be modeled by smoothed step functions. In other words, the reaction rate dg_i/dt has a Gaussian evolution and it is maximal at the center of the interval ($g_i = 0.5$).

2.2.2 Thermophysical properties

The density of resin compound decreases as water is released during degradation according to the following relationship:

$$\rho_r = \rho_{r0}(1 - f_w) \quad (1)$$

where $\rho_{r0} = 1800 \text{ kg.m}^{-3}$ is the initial density of non-degraded resin compound and f_w is the mass fraction of released water ($0 < f_w < 0.225$) (IRSN/AREVA internal report, 2013). An average porosity value $P = 0.1$ is assumed as a first approximation, but one should note that this parameter is not known precisely and its influence on the model results could be analyzed. The heat capacity and the thermal conductivity of resin compound are given as functions of temperature in **Table 1**. Below and over the extremum temperatures, the heat capacity and thermal conductivity values are extrapolated as constant.

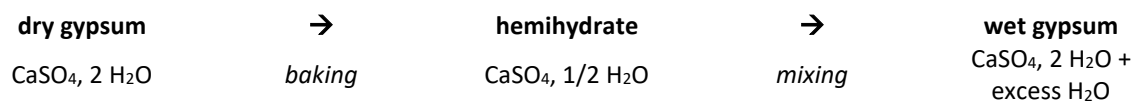
2.3 Plaster

Plaster is an inorganic porous material that consists of calcium sulphate (CaSO_4) in more or less hydrated states:

- gypsum (dihydrate): $\text{CaSO}_4, 2 \text{H}_2\text{O}$ (+ possible excess of water);
- plaster (hemihydrate): $\text{CaSO}_4, \frac{1}{2} \text{H}_2\text{O}$;
- anhydrite: CaSO_4

Plaster is an effective thermal protection material for transportation casks because it contains within its pores a certain amount of water, which absorbs a large part of the thermal energy of the fire while vaporizing. Moreover, it exhibits two phase transitions, respectively around 145 °C and 210 °C, which also participate in the absorption of energy. For these reasons, similar water vapor transport phenomena as in polymer resin compound are likely to occur.

Plaster is obtained from natural gypsum ($\text{CaSO}_4, 2 \text{H}_2\text{O}$) through two inverse transformations: gypsum is first partially dehydrated by baking in an oven then the addition of excess water (mixing) leads to the formation of a paste, which is chemically identical to gypsum and hardens when exposed to air:



The water remains trapped in the pores of the plaster microstructure and can be removed by drying, although it is generally preserved (improves fire protection because of slower heat transfer). The mixing ratio (denoted G) is the amount of water, in kg, added per kg of hemihydrate. This parameter is very influential because the amount of excess water determines the structural porosity of the plaster after setting. It therefore affects all thermophysical properties. After mixing and setting, wet gypsum can be partially dried, that is, a fraction of the free water contained in the porosities has evaporated and replaced by air. The moisture content (denoted by τ , with $0 < \tau < 1$) represents the fraction of free water actually contained in the porosities in relation to the total volume of porosities filled by water.

2.3.1 Dehydration reactions

During a temperature rise, the wet gypsum (initial state) undergoes 3 successive endothermic reactions (IRSN/AREVA internal report, 2013), during which water vapor is released (**Figure 3**):

- vaporization of the excess water between 100 ° C and 105 ° C : reaction R1, $\Delta H_{\text{vap}} = -2257 \times 10^3 \text{ J.kg}^{-1}_{(\text{H}_2\text{O})}$;
- transformation of the dihydrate (dry gypsum) into hemihydrate with evaporation of the released water between 115 ° C and 175 ° C: reaction R2, $\Delta H_{\text{R2}} = -565 \times 10^3 \text{ J.kg}^{-1}_{(\text{CaSO}_4, 2\text{H}_2\text{O})}$
- transformation of the hemihydrate to anhydrite with evaporation of the released water between 200 ° C and 220 ° C: reaction R3, $\Delta H_{\text{R3}} = -233 \times 10^3 \text{ J.kg}^{-1}_{(\text{CaSO}_4, 1/2\text{H}_2\text{O})}$

Each reaction is assumed to be uniformly distributed over its entire temperature range. As a result, their advancement (value between 0: reaction not started and 1: reaction completed) can be described by linear functions of temperature. Consequently, the evolutions of plaster properties between 2 stable states are also described by linear functions of temperature

2.3.2 Thermophysical properties

The thermophysical properties of the stable states of plaster are summarized in **Table 2**. The analysis of the molar masses of the different components in the stable states of plaster in stoichiometric proportions leads to density expressions as functions of the mixing ratio G and the moisture content τ . Note that the optimal mixing ratio value $G_{\text{opt}} = 0.186$ corresponds to the case of no excess water (total mixing reaction). Between the stable states, the density of the plaster is assumed to follow a linear evolution with temperature, bounded by the density values of the adjacent stable states. Moreover, the potential porosity is defined as the volume occupied by the excess water after mixing for $\tau = 1$:

$$P = \frac{(G - 0.186) \frac{2750}{1 + 2.75G}}{1000} = (G - 0.186) \frac{2.75}{1 + 2.75G} \quad (2)$$

This expression is only valid for a sufficiently mixed plaster *i.e.* for $G \geq 0.186$.

The heat capacity values as well as the mass fractions of the different plaster states are given by linear functions of temperature. The heat capacity expression of wet gypsum takes into account the presence of excess water in variable amount that depends on the mixing ratio G and on the moisture content τ . Again, between the stable states, the heat capacity of the plaster is assumed to follow a linear evolution with temperature, bounded by the heat capacity values of the adjacent stable states.

For thermal conductivity, a parallel law as a function of the porosity P is used. For wet gypsum ($T < 100$ °C), it is assumed that the porosities are filled with water at a moisture content τ and air for $(1 - \tau)$. For dry gypsum and subsequent states ($T > 105$ °C), it is assumed that the porosities are totally dry, thus completely filled with air ($\tau = 0$). The conductivity value of the solid plaster matrix is estimated as $k_{\text{matrix}} = 0.35 \text{ W}\cdot\text{m}^{-1}\cdot\text{K}^{-1}$. During the evaporation of excess water (reaction R1), the thermal conductivity of the plaster follows a linear evolution with temperature between the thermal conductivity values of the wet gypsum and dry gypsum.

2.4 High density phenolic foam

Phenolic foam is a cellular material resulting from the foaming and crosslinking of a phenol-formaldehyde (or phenolic) thermosetting resin. Besides its remarkable mechanical properties, rigid phenolic foam constitutes a very interesting shielding material for cask walls thanks to its very good fire behavior (little or no flame spread, negligible emission of black and toxic smokes, no melting or liquefaction in the presence of a heat source) and its excellent thermal insulation properties due to a closed cell porous structure with very small cell diameter. Phenolic foams are produced with a wide range of densities (from a few tens to a few hundred kg/m^3), depending on the application (simple thermal insulation or structural function). The foams of interest for the present application are high density foams: about $500 \text{ kg}/\text{m}^3$. When exposed to the high temperatures of a fire, phenolic foam undergoes thermal degradation without flame (pyrolysis) which is accompanied by gaseous releases, in particular water vapor. As for polyester resin compound and plaster, in a confined environment, evaporated water is likely to diffuse and recondensate in neighboring colder areas. This condensation is accompanied by a gain of latent energy by the material.

2.4.1 Degradation reactions

Since a complete and comprehensive dataset for a specific sample of phenolic foam could not be obtained from the literature, this paper attempts to synthesize the information available from various sources using a number of assumptions, in order to model a typical thermal behavior of phenolic foam. Complementary data have been found in the works of Chang and Tackett (Chang and Tackett, 1991) and Lee (Lee, 2007), which investigate thermal decomposition of phenolic resins by thermogravimetric analysis - mass spectroscopy (TG-MS). The results include the fraction of mass loss attributed to the release of water as well as the temperatures at which these releases occur, which is essential information for the present study. The total enthalpy of reaction of the foam was determined for a sample of "FENO 5" foam (LNE/AREVA internal report, 2009) by simultaneous measurements of the heat flow absorbed by the sample and the mass loss using a cone calorimeter. The nominal value determined is $\Delta H_r = 15544$ kJ/kg. This value corresponds to all the reactions undergone by the material between the beginning and the end of its degradation, hence the fraction of this enthalpy which corresponds solely to the release of water vapor and the released amount of water vapor are not known beforehand. To the best of our knowledge, such quantitative data is not available in the open literature. Nevertheless, experimental results (Chang and Tackett, 1991),(Lee, 2007) are available for a sample of phenolic resin, which can be assimilated to the solid phase (matrix) of phenolic foam. These data are summarized in **Table 3**. Summing the respective mass losses of the three phases considered in the table, it is deduced that the complete degradation of a phenolic resin leads to the release of 16% of its initial mass as water vapor. The advancement $g(T)$ of the overall degradation reaction is given versus temperature in **Table 4**.

This overall advancement function is used to calculate the volumetric power absorbed by the medium during thermal degradation:

$$Q_R = -\rho_m \Delta H_r \frac{dg}{dt} \quad (3)$$

where ρ_m is the density of the phenolic foam. The advancement degree of the water vapor release phases is modeled by three smoothed step functions $g_{vi}(T)$ ($i = 1$ to 3), with $0 < g_{vi} < 1$, corresponding to the temperature ranges described in **Table 3**. The mass of water vapor released per unit mass of foam for each phase are as follows:

- $g_{v1} : 90^\circ\text{C} \rightarrow 104^\circ\text{C} \quad m_1 = 0.008 \rho_{m0} \text{ (kg/m}^3\text{)}$
- $g_{v2} : 104^\circ\text{C} \rightarrow 270^\circ\text{C} \quad m_2 = 0.044 \rho_{m0} \text{ (kg/m}^3\text{)}$
- $g_{v3} : 270^\circ\text{C} \rightarrow 600^\circ\text{C} \quad m_3 = 0.107 \rho_{m0} \text{ (kg/m}^3\text{)}$

where ρ_{m0} is the initial density (i.e. before any degradation) of the foam.

In addition, the following assumptions are considered for the three endothermic materials:

- in case of recondensation, vaporized water does not modify the properties of the material region in which it recondensates;
- degradation reactions are irreversible: if temperature in a given material region decreases, the thermophysical properties of this region are fixed at the values corresponding to the maximum temperature reached;
- the volume of the endothermic material domain remains constant during the successive degradation reactions, but the mass included in the domain changes according to the density function of the material.

2.4.2 Thermophysical properties

The studied typical phenolic foam has an initial density $\rho_{f0} = 500 \text{ kg.m}^{-3}$. The density versus temperature evolution can be modeled by referring to TG results by means of a (irreversible) mass loss function $f_m(T)$ such that:

$$\rho_f = f_m(T) \rho_{f0} \quad (4)$$

The mass loss function adopted in the present model is given versus temperature as shown in **Table 5**.

The porosity of the foam is defined as the volume of gas contained in a unit volume of foam, thus neglecting the density of the gas with respect to that of the solid matrix:

$$P = 1 - \frac{\rho_{f0}}{\rho_m} \quad (5)$$

where ρ_m is the density of the phenolic resin constituting the matrix. A standard value of $\rho_m = 1100 \text{ kg.m}^{-3}$ is considered, which leads to $P = 0.545$. The heat capacity of the "FENO 5" phenolic foam was characterized at near-ambient temperatures (LNE/AREVA internal report, 2009) and is given in **Table 6**. The thermal conductivity of the "FENO 5" foam was characterized using the guarded hot plate method at an average temperature of 20 °C. The value obtained is: $k_m = 0.115 \text{ W.m}^{-1}.\text{K}^{-1}$. As a first approximation, the thermal conductivity will be considered as constant and independent of temperature.

2.5 Other materials

The gap corresponding to the clearance between the solid parts (metallic fin and shielding material) consists of air in which the water vapor can diffuse. Also, within the porous shielding material, air is present in the gas phase. As a first approximation, the density of air is approximated as the density of dry air and calculated according to the ideal gas law. The heat capacity and the thermal conductivity of air are described as functions of temperature (Incropera et al., 2002). The mutual diffusion coefficient of water vapor in air is assumed to be temperature-dependent, according to the following equation (Mchirgui, 2012) :

$$D_{w/air} = 0.26 \times 10^{-4} \left(\frac{T}{298} \right)^{\frac{3}{2}} \quad (6)$$

Natural convection is assumed to be negligible in the gas phase. Moreover, the aerodynamic pressure gradient in the gas phase is assumed to be very low: forced convection is also considered as negligible.

Hence, diffusion of water vapor in air (and associated latent heat) is the only assumed mechanism of heat and mass transfer in the interstices.

The stainless steel constituting the outer and inner shells has the following thermophysical properties, supposed to be independent of temperature: density $\rho_{ss} = 7920 \text{ kg.m}^{-3}$, heat capacity $C_{p,ss} = 520 \text{ J.kg}^{-1}.\text{K}^{-1}$, thermal conductivity $k_{ss} = 17 \text{ W.m}^{-1}.\text{K}^{-1}$.

The copper constituting the heat dissipation radial fins has the following thermophysical properties, supposed to be independent of temperature: density $\rho_{Cu} = 8930 \text{ kg.m}^{-3}$, heat capacity : $C_{pCu} = 390 \text{ J.kg}^{-1}.\text{K}^{-1}$, thermal conductivity : $k_{Cu} = 400 \text{ W.m}^{-1}.\text{K}^{-1}$.

3 Finite Element Model

This section introduces the assumptions, equations and boundary conditions used to set up the finite element model of coupled heat and mass transfer within the different parts of the cask wall section.

3.1 Domain equations

Conduction heat transfer in the shielding material domain is modeled by the heat diffusion equation (Incropera et al., 2002) with a heat sink term Q_R (volumetric power, W/m^3) corresponding to the latent heat absorption associated with the endothermic decomposition reactions and a heat source term Q_{cond} corresponding to the latent heat released by water and recovered by the shielding material during recondensation:

$$\rho C_p \frac{\partial T}{\partial t} + \nabla \cdot (-k \vec{\nabla} T) = Q_R + Q_{cond} \quad (7)$$

The volumetric power Q_R is composed of several contributions Q_{Ri} corresponding to the various reactions i occurring in the material:

$$Q_R = \sum_i Q_{Ri} \quad (8)$$

with:

$$Q_{Ri} = -\rho \Delta H_i \frac{dg_i}{dt} \quad (9)$$

ΔH_i is the transformation enthalpy (in J/kg of material) of reaction i and g_i is the degree of advancement of reaction i . Thus, the heat absorption rate of reaction i is proportional to the reaction rate. The volumetric power returned to the shielding material during condensation is given by:

$$Q_{cond} = -R_{cond} M_w \Delta H_{cond} \quad (10)$$

where R_{cond} is the mass source term (in mol/(m³.s)) corresponding to the water vapor condensation in the shielding material, $M_w = 18$ g/mol is the molar mass of water and $\Delta H_{cond} = 2257$ kJ.kg⁻¹ is the latent heat of condensation of water.

Diffusion mass transfer of water vapor into the porous medium is modeled by Fick's law (Mchirgui, 2012) with mass source terms, in transient form. This equation expresses the conservation of the quantity of water. The diffusive flux of water vapor in the air of the pores is proportional to the gradient of the water content of the air contained in the pores:

$$\frac{\partial c_w}{\partial t} + \nabla \cdot (-D_{eff} \vec{\nabla} c_w) = R_{vap} + R_{cond} \quad (11)$$

where c_w is the water content of air (expressed as a volumetric molar concentration, mol/m³) and D_{eff} is the effective diffusivity of water vapor in the porous medium. The rate of generation of the water vapor produced by the reactions is modeled by the (positive) source term R_{vap} (in mol/(m³.s)), which is the sum of all the contributions from the various reactions i :

$$R_{vap} = \sum_i R_{Ri} \quad (12)$$

where

$$R_{Ri} = \rho \frac{m_{wi} dg_i}{M_w dt} \quad (13)$$

m_{wi} represents the total mass of water which can be released per unit mass of material during reaction i and g_i is the degree of advancement of reaction i . The mass loss corresponding to the condensation of water vapor in the porous medium is modeled by the (negative) source term R_{cond} :

$$R_{cond} = -k_{cond}(T_{cond} - T)c_w \quad (14)$$

where k_{cond} is the condensation coefficient (K⁻¹.s⁻¹). Its value is not known beforehand, it should be chosen so that the solution is not significantly affected if it is further increased. This amounts to assuming that the vapor is in equilibrium with the liquid, in other words that the characteristic time of the condensation process is very small in front of the characteristic diffusion time. The value of k_{cond}

affects the width of the condensation zone (the higher its value, the narrower the zone, because the more instantaneous the process). In this work, an intermediate value $k_{cond} = 0.1$ is adopted. The condensation temperature T_{cond} is assumed to be 100 °C. Moreover, it is assumed that condensation is irreversible: the water mass already condensed once cannot vaporize again. Mathematically speaking, this mass disappears from the model. Indeed, if taken into account, the effect of this phenomenon on heat transfer would be negligible: the secondary vaporization and recondensation taking place at the same temperature, vapor would diffuse over a distance so small that there would be no effective increase of heat transfer. This is all the more true as the characteristic time of the condensation process is smaller than the characteristic time of the diffusion process.

In order to characterize the diffusion of water vapor in a porous medium with a solid matrix such as the investigated shielding materials, one of the simplest and most efficient approaches consists in considering the effective diffusivity of water vapor in the porous medium (Halder et al., 2011):

$$D_{eff} = \frac{\varepsilon_p}{\tau_L} D_{w/air} \quad (15)$$

According to this expression, the influence of the structure of the porous medium on the diffusivity value is described by two dimensionless parameters:

- porosity ε_p , which is the volume ratio of pores in the medium;
- tortuosity τ_L , which characterizes the ratio of the actual length of the path traveled across a representative volume element of the porous medium while passing exclusively through the pores to the length of the path traveled across it in a straight line.

Several models exist to link tortuosity to porosity. Basically, tortuosity decreases as porosity increases. The most commonly used model has been proposed by Millington & Quirk (Millington and Quirk, 1961):

$$\tau_L = \varepsilon_p^{-1/3} \quad (16)$$

According to this approach, which is satisfying as a first approximation, the only independent parameter is porosity. The advantage of this model is that porosity can be easily estimated by mass measurements, whereas a more sophisticated approach would require detailed morphological characterization of the pore structure.

In the domains constituted of metallic materials (outer and inner shells, radial fin), conduction heat transfer is simply modeled by the heat diffusion equation without heat source term:

$$\rho C_p \frac{\partial T}{\partial t} + \nabla \cdot (-k \vec{\nabla} T) = 0 \quad (17)$$

Neither mass transfer nor phase change phenomena occurs in these domains.

Diffusion mass transfer of water vapor in the air of the interstice is modeled by Fick's law in transient form, indicating that the diffusive flux of water vapor is proportional to the gradient of the water molar concentration in air c_w :

$$\frac{\partial c_w}{\partial t} + \nabla \cdot (-D_{w/air} \vec{\nabla} c_w) = R_{cond} \quad (18)$$

$D_{w/air}$ is the diffusivity of water vapor in air. The vapor can also disappear by condensation in the air of the interstice or on the surrounding walls with the mass loss rate R_{cond} :

$$R_{cond} = -k_{cond}(T_{cond} - T)c_w \quad (19)$$

Heat transfer in the air gap is modeled by the heat diffusion equation with the heat source term

Q_{cond} corresponding to the condensation of water vapor.

$$\rho C_p \frac{\partial T}{\partial t} + \nabla \cdot (-k \vec{\nabla} T) = Q_{cond} \quad (20)$$

$$Q_{cond} = -R_{cond} M_w \Delta H_w \quad (21)$$

Convection is assumed to be a negligible heat transfer process in this domain.

3.2 Boundary conditions

The conditions applied at the boundaries of the material domains are summarized in **Figure 4**.

Wherever no boundary condition is explicitly specified for a given boundary, the assumed boundary condition is continuity of fluxes and field variables (temperature or concentration). The heat flux

exchanged between the environment and the outer shell is modeled by a convective and ambient radiation boundary condition. The environment (including the fire) and the outer surface of the shell are considered as gray surfaces: their emissivity and their absorptivity are assumed to be equal at all times. The net heat flux representing the heat transfer between the surface of the outer shell (temperature T_s) and the environment (temperature T_{amb}) is therefore given by:

$$q''_s = F_{fs}\sigma(T_{amb}^4 - T_s^4) + h(T_{amb} - T_s) \quad (22)$$

where $\sigma = 5.68 \times 10^{-8} \text{ W.m}^{-2}.\text{K}^{-4}$ is the Stefan-Boltzmann constant, $h = 10 \text{ W.m}^{-2}.\text{K}^{-1}$ is the convective heat transfer coefficient (free convection). The thermal coupling between the fire (emissivity ε_f) and the surface of the outer shell (emissivity ε_s) is represented by the coupling factor:

$$F_{fs} = \frac{\varepsilon_f \varepsilon_s}{1 - (1 - \varepsilon_f)(1 - \varepsilon_s)} \quad (23)$$

The temperature of the radiative heat source is given as a function of time (fire phase, cooling phase):

$$\begin{aligned} 0 < t \leq t_f & : T_{amb} = 1073.15 \text{ K} \\ t > t_f & : T_{amb} = 311.15 \text{ K} \end{aligned} \quad (24)$$

where $t_f = 1800 \text{ s}$ is the duration of the fire.

The inner surface of the inner shell is supposed to be insulated (zero flux), i.e. heat is not transferred to the air volume included inside the cavity, which is a conservative assumption. The thermal condition between the outer shell and the shielding material is represented by a thermal resistance R_c ($\text{m}^2.\text{K}/\text{W}$) whose value changes over time to take account of the formation of an air gap of thickness e_{air} , due to the degradation of the material located in the superficial layer beneath the outer shell:

$$R_c = \frac{e_{air}}{k_{air}} \quad (25)$$

The thickness of the air layer changes as follows: during the fire phase ($t \leq t_f$), $e_{air} = 0$; during the cooling phase ($t > t_f$), $e_{air} = 10 \text{ mm}$. This assumption allows taking into account in a penalizing manner the influence of the material degradation, which slows down the cooling of the cask. This boundary is also assumed to be impermeable to mass transfer (zero mass flux).

3.3 Numerical methods

The finite element method (FEM) implemented in COMSOL Multiphysics software is used to solve the model. The mesh consists of triangular elements with quadratic interpolation functions. The total number of elements is around 16500. The model is solved in a transient analysis from $t_0 = 0$ to $t_{end} = 15000$ s. The time step is variable and self-adaptive depending on the dynamical evolution of the system and the numerical convergence. Thus, during the vaporization and condensation phases, a very small time step is adopted.

4 Results and Discussion

The simulations yield the evolution of the temperature and the diffusive water vapor flux fields in the wall, as well as the field of the water vaporization and condensation rates, during the fire and cooling phases. The temperature evolutions at any selected point can be deduced from the temperature field.

4.1 Temperature field

The temperature field in the wall is shown for several times of the fire phase, for the three investigated shielding materials in **Figure 5**. The minimum and maximum temperatures at each time are also indicated. The conductive role of the copper fin appears clearly and results in a significant temperature inhomogeneity in the outer shell with the presence of a cold spot on the fin-side symmetry plane and a hot spot at the opposite symmetry plane. At the end of the fire phase, the maximum temperature difference predicted in the outer shell is about 230 °C in the case of resin compound as shielding material, 300 °C in the case of plaster and 200 °C in the case of phenolic foam. The same phenomenon occurs in a reverse way on the inner shell: a hot spot on the fin-side symmetry plane and a cold spot on the opposite symmetry plane. The maximum temperature difference is about 250 °C in the case of resin compound as shielding material, 225 °C in the case of both plaster and phenolic foam. The maximum temperature at the end of the fire phase is located on the outer surface of the outer shell, on the symmetry plane opposite to the fin side. Note that the shielding material is heated both from the outer shell and the fin (despite the air gap separating them) which results in non-circumferential

isotherms. For identical configuration and boundary conditions, the temperature gradients are clearly greater in the case of the phenolic foam wall than in the case of plaster and resin compound walls. Indeed, among the three studied materials, the phenolic foam is the one with the best insulating properties. On the contrary, the temperature field in the polyester resin compound wall is smoother since overall heat transfer is better in this material.

4.2 Temperature evolutions

The time evolutions of temperature along the symmetry mid-plane of the cask wall have been plotted in **Figure 6**, **Figure 7** and **Figure 8** for the locations indicated in **Figure 4**. The exact locations are as follows (with e_s : thickness of the shielding material): P1.1: outer surface of the outer shell; P1.2: inner surface of the outer shell; P1.3: $e_s/4$; P1.4: $e_s/2$; P1.5: $3e_s/4$; P1.6: outer surface of the inner shell; P1.7: inner surface of the inner shell. The evolutions calculated with the “full” model (*i.e.* taking into account heat conduction, latent heat release due to decomposition reactions and latent heat absorption due to vapor recondensation) are compared with the results yielded by a much simpler “conduction-only” model (which only accounts for heat conduction inside the wall).

For the three investigated materials, the conduction-only model results in higher overall temperatures than the full model. This is due to the fact that for the latter, the amounts of heat of reaction and latent heat absorbed during thermal degradation and water vaporization are not returned integrally to the material by condensation during the fire phase. Only a fraction of the latent heat of vaporization is restored during the condensation of the water vapor. This necessarily leads to a “loss of energy” of the model and therefore to lower temperatures. Also, the full model (including gaseous transfer phenomena) exhibits a steep initial temperature increase at the beginning of the fire phase, then a sudden slowing down of this evolution (inflection point). This behavior is not observed for the conduction-only model, for which the temperature evolutions are much more regular.

Figure 9, **Figure 10** and **Figure 11** show more clearly the comparison of the temperature evolutions in the shielding layer and in the inner shell, calculated by both models, for the three investigated materials. For both polyester resin compound and plaster, it is quite clear that the temperature

increase up to 100 °C is much faster in the case of the model including reactions and gas transport. Over 100°C, the heating kinetics slows considerably and the temperatures eventually become lower than those resulting from the conduction-only model. This increase in heat transfer can be related to the diffusion of vapor in the porous medium: the latent heat absorbed in the reaction zones would then be transported to the condensation zones (where it is returned to the material) more rapidly than sensible heat transferred by conduction. Moreover, in the model, the threshold value of condensation temperature has been assumed as 100 °C. It therefore seems coherent that as soon as the material temperature exceeds this threshold value, this heat transfer intensification recedes (since latent heat is no longer restored). For phenolic foam, contrary to what is observed for resin compound and plaster, the model including reactions and gas transport leads to both lower temperature levels and slower thermal kinetics than the conduction-only model. The accelerating effect of the temperature rise at the beginning of the fire phase that was attributed to the heat transfer intensification mechanism by gas diffusion for the other materials is not observed here. This could mean that:

- for phenolic foam, the fraction of enthalpy of reaction corresponding to the vaporization of water is small compared to the total value of this enthalpy of reaction. Therefore, the major part of the heat absorbed is never returned to the material, which would explain the significant temperature differences between the results of the two models;
- the vapor diffusion mechanism in the porosities of the phenolic foam is not significant compared to the conductive transfer in the solid matrix, which could be explained by small amounts of water vapor released (temperatures reached are too low), by a high resistance to vapor diffusion, as well as by recondensation zones being located very close to the vaporization zones.

4.3 Analysis of gas transport phenomena: vaporization, diffusion and condensation of water vapor

In order to confirm and precisely explain the effects mentioned in the previous section, it is necessary to analyze the water vapor transfer phenomena in the endothermic material. **Figure 12** shows the

simulated field of the water vapor mass source / mass sink term (unit: $\text{mol}\cdot\text{m}^{-3}\cdot\text{s}^{-1}$), *i.e.* the areas where water vaporization occurs (positive value: mass source) and where recondensation occurs (negative value: mass sink), at several times during the fire phase. The value denoted "max" corresponds to the maximum vaporization rate and the value denoted "min" to the maximum condensation rate. The color scale is variable in terms of its extrema, but it is always symmetrical: the light green color always corresponds to a zero rate (*i.e.* no reaction). The blue zones correspond to the reaction fronts and the red zones to the condensation front. The mass flux of water diffusing through the porous material and into the air gap is represented by the vector field. The length of the arrows is proportional to the norm of the mass flux density vector (unit: $\text{mol}\cdot\text{m}^{-2}\cdot\text{s}^{-1}$). The plots clearly show the three vaporization fronts that correspond to the successive decomposition reactions assumed for the considered materials (labeled "R1", "R2" and "R3") and the condensation front, labeled "C". Logically, in the zone located between the vaporization fronts and the condensation front, a diffusive flux of water vapor is established. The mass flux generated by the different fronts are additive, as shown by the variation in the size of the arrows. One note a significant flux magnitude in the air gap between the resin compound and the fin, which is explained by an effective diffusion coefficient much higher in air than in the porous materials. However, in the air gap, the cross-section of passage is much smaller than in the solid wall. In the case of polyester resin compound, the condensation front reaches the inner shell before the end of the fire phase (at $t = 1200$ s) and the minimum value of the mass creation rate becomes zero, which means that the conditions necessary for condensation are no longer verified at any point in the wall: the vapor formed is no longer condensed. According to the assumptions of the model, the vapor then accumulates in the air volumes present in the resin compound and in the interstice. The water vapor concentration gradient then begins to decrease and the diffusive flux tends to vanish. From an energy point of view, it is recalled that the "R" zones correspond to latent heat absorption from the material and that the "C" zone corresponds to latent heat return to the material. Therefore, the latent heat transport between these two types of zones leads to the enhancement of the global heat transfer because in the present case, mass diffusion is faster than heat conduction. On the other hand, as soon

as the "C" zone vanishes, latent heat is no longer restored to the material and the enhancement effect recedes. This is consistent with the temperature evolutions shown in **Figure 6** and **Figure 9**. Similar observations can be made in the case of plaster, however, the reaction and condensation fronts progress much more slowly towards the inner shell than for PE resin compound. Hence, the distances between the fronts are smaller and so is the vapor diffusion distance. Moreover, the condensation front does not reach the inner shell during the fire phase. This explains that the heat transfer enhancement effect is less acute and does not extend to the inner region of the plaster wall, as seen in **Figure 10**. For phenolic foam, the condensation front progresses only on a very short distance in the direction of the inner shell and remains very close to the reaction fronts. This is related to the low thermal diffusivity of the phenolic foam, which does not allow fast heat propagation into the material. Hence, the latent heat transfer cannot occur on a sufficient radial distance and it is not significant compared to the conductive heat transfer. In addition, the magnitude of the mass source term (which reflects the importance of the latent heat amounts involved) remains low compared to what had been calculated for resin compound and plaster (about 10 times lower). Indeed, the amounts of water vapor transferred by diffusion in phenolic foam remain much lower than those involved in the materials previously studied. This explains why no acceleration of the temperature rise in the foam and at the inner shell is observed with respect to the prediction of the conduction-only model (**Figure 11**). It can therefore be concluded that for phenolic foam, given the assumptions made on the material data, gas diffusion heat transfer remains insignificant compared to conductive heat transfer.

In summary, it appears that the integration of this additional heat transfer mode in the simulation leads to very consistent results from the phenomenological and qualitative point of view, specially concerning the effect on the heat transfer kinetics in the material. The importance of these phenomena strongly depend on the physicochemical nature of the material. Plaster is a mineral material in whose composition water enters in substantial proportion will be subject to significant amounts of vapor released at relatively low temperatures, maximizing the potential for recondensation of this vapor. On the other hand, an organic thermosetting material such as phenolic

foam is subjected to degradation reactions producing their greater amounts of water vapor at higher temperatures, which tends to delay and reduce gas transfer and the thermal kinetics acceleration effect produced by recondensation. In addition, the distance between the vaporization zones and the recondensation zones must be significant relative to the wall thickness for this phenomenon to be effective. This distance is conditioned both by the temperatures at which the material is likely to release vapor and by the temperature gradient in the wall, therefore by the thermal diffusivity of the material. However, due to a number of simplifying assumptions and lack of data concerning the model parameters, quantitative accuracy is certainly not optimal. In the following sections, the influence of two not precisely characterized parameters on the model predictions is analyzed:

- the porosity of the material: a parameter governing the effective diffusivity of the porous medium;
- the condensation coefficient, a parameter governing the ratio between the characteristic times of vapor diffusion and condensation, which can play an important role on the thermal kinetics.

4.4 *Influence of the porosity parameter*

In the present model, the porosity parameter of the material is expected to have significant influence on the intensity of gas transport predicted by the simulation. Actually, porosity is rather low for non-degraded materials and increases with thermal degradation and pyrolysis. However, the relationship between degradation and porosity being difficult to characterize in a quantitative way for each of the studied materials, the model assumes that porosity is homogeneous and constant. In order to assess the impact of this assumption as well as obtain limiting cases behavior corresponding to undegraded and very degraded material conditions, the sensitivity of this porosity parameter on the temperature evolutions of the inner shell has been analyzed. The simulations have been carried out for the case of polyester resin compound as shielding material. Porosity values ranging from 1% to 50% have been investigated. This upper bound value is rather unrealistic for the present resin compound in

undegraded condition (rather corresponding to the porosity of a light foam), but it should be considered as a limiting case which could represent a very degraded material. This sensitivity analysis allows to circumscribe the actual thermal behavior of the wall (*i.e.* increasing porosity in the degraded regions during the fire test) and thus assess the influence of this porosity parameter on the temperature inside the cask cavity.

The evolution of the temperature at the extremum points I and II as well as the average temperature are shown in **Figure 13**, for the different values of porosity. Recall that the results obtained in the previous section were obtained using a porosity value of 0.1. The results of the conduction-only model calculation are also shown in dashed lines. For porosity values between 5% and 50%, the variability remains rather low: the heating kinetics are very similar, as well as the reached temperature levels. On the other hand, for the lowest porosity value (1%), the heating kinetics is significantly slowed down: a time offset of 200 s is observed at point I, as well as a moderate temperature difference (about 5K). Indeed, the Millington & Quirk tortuosity model (Millington and Quirk, 1961) used here, Eq. (16), predicts that tortuosity becomes very high when porosity tends to zero. Logically, according to Eq. (15), this also results in the effective diffusion coefficient becoming quite low: vapor can then hardly diffuse into the porous medium and latent heat transfer is negligible. Conversely, when porosity increases, tortuosity tends to an asymptotic value of zero, which corresponds physically to “straight line” diffusion. The effective diffusion coefficient is then only influenced by the reduced diffusion section effect and should tend to the value of the diffusivity of water in air. This explains why the influence of porosity seems important only in the low value range (below 5%), for which tortuosity is a significant parameter. Beyond this value, the thermal behavior remains rather consistent and only affected linearly by the diffusion section.

4.5 Influence of the condensation coefficient

The mass transfer model assumes that the condensation rate of water vapor (in mol H₂O/(m³.s)) is given by Eq. (14). In this expression, the term denoted k_{cond} is a numerical coefficient that quantifies

the characteristic time of the condensation process. When compared to the characteristic time of diffusion of the vapor in the porous medium (governed by the effective diffusion coefficient), it allows determining if the limiting process of the latent heat transfer is condensation (low k_{cond} value) or diffusion (high k_{cond} value). The condensation coefficient is an adjustable parameter of the model. As such, the limit case values can be determined by assuming arbitrary values and examining a particular result, for instance, the calculated temperature evolutions. If the results don't change significantly as the value is lowered (resp. raised), then the lower (resp. upper) bound is obtained. In the simulations presented in the previous sections, it has been assumed that condensation is an instantaneous process with respect to diffusion, *i.e.* diffusion is the limiting process (intermediate value $k_{cond} = 0.1$). This explains the narrow appearance of the predicted condensation fronts: as soon as the vapor enters an area where condensation is possible, it condenses instantly. If the condensation coefficient is lower, it tends to a situation where condensation can no longer be considered instantaneous: at a given point, there is a limitation (or saturation) effect of the condensation rate. A fraction of the non-condensed vapor then continues diffusing beyond this point until reaching an area where the condensation rate is not yet maximum. This should lead to a more spread appearance of the condensation front.

The influence the condensation coefficient on the temperature evolution of the inner shell is shown in **Figure 14**. The appearance of the condensation front and the distribution of the vapor diffusive flux of are represented, for time $t = 400s$, in **Figure 15**. This parametric study has been carried out in the case of PE resin compound as wall material. For a very low k_{cond} value of 10^{-6} , the vapor generated diffuse under the effect of the concentration gradient, but recondenses extremely slowly: there is latent heat absorption from the material, but only a small fraction of this latent heat is finally restored to the material. As a result, the temperature evolution curves show a very slow increase and reach lower temperature levels. This case seems physically unrealistic (extremely long condensation compared to diffusion), but illustrates well a theoretical asymptotic trend of the model. For $k_{cond} = 10^{-4}$, the temperature levels reached are much higher: it can be deduced that the amount of latent heat returned to the material is globally equivalent to that of the reference case (instantaneous

condensation). Moreover, from the thermal kinetics point of view, the increase in internal shell temperature is even slightly faster than for the reference case. This result is surprising, but can be explained by the fact that the condensation front is quite wide: condensation occurs earlier in the vicinity of the resin / inner shell interface, thus the contribution of latent heat is perceptible. This case is more physically realistic and corresponds to characteristic times of diffusion and condensation of the same order of magnitude. From $k_{cond} = 10^{-2}$ and above, the trend is asymptotic: as k_{cond} increases, temperature levels and thermal kinetics tend to be very similar. Condensation fronts become relatively narrow and localized. A clear slope inflexion appears on the temperature evolution curves. Instantaneous condensation is the dominant process.

The influence of the condensation coefficient is therefore clearly noticeable and meaningful. This parameter of the model seems to play an important role on the shape of the temperature evolution curves obtained and will have to be considered with attention in case of model validation against experimental data. If the unrealistic values are discarded, a practical value ranging from 10^{-4} (slow condensation) to 1 (instantaneous condensation) can be assumed. The shape of the experimental temperature curves (sharpness of the slope inflexion) should allow to approach the actual value. However, one should note that for a value chosen in this range, the variability of the results remains limited, which brings credit to the robustness of the model with respect to this parameter.

5 Conclusion

This paper describes a possible strategy for modeling the phenomena that may affect the thermal performance of a transportation cask under accidental fire conditions. The model is based on detailed and explicit consideration of the physical phenomena of mass and heat transfer (heat conduction, vaporization of the hydrated load, fickian diffusion in a porous medium, condensation) using the main physical parameters related to the material: thermophysical properties, heat of reaction, porosity, tortuosity, condensation coefficient. Although not all of these parameters are known precisely and a certain number of assumptions have to be formulated (especially in the case of phenolic foam wall, which might lead to some uncertainty in the results), the model ultimately yields very consistent

qualitative and quantitative predictions of thermal variables and allows good understanding of the influence of the dehydration reaction phenomena on heat transfer.

It has been shown that a simplified conduction-only model significantly and consistently overestimates the temperature levels compared to a more detailed model taking into account degradation reactions, water vapor diffusion and recondensation. This could be explained by the fact that the latent heat absorbed from the material during decomposition reactions (endothermic) is not fully restored during recondensation (exothermic). Indeed, the temperature conditions in the wall subjected to fire are such that any recondensation becomes impossible before even all the water vapor is released by the successive decomposition reactions. The simplified model does not account for this latent heat loss to the exterior of the system, hence the global overestimation of the temperature levels reached. The increase in internal pressure due to vapor accumulation is expected to reduce this energy loss (by increasing condensation temperature) and lead to higher temperature levels.

Moreover, it has been shown that taking into account the gas transport phenomena leads to enhancement of the predicted heating kinetics of the inner shell compared to the predictions of the simplified model. This observation has to be nuanced according to the endothermic material considered. The acceleration effect is quite noticeable for the cases of polyester resin compound and plaster as shielding materials, however it has not been clearly evidenced in the case of the phenolic foam wall. This difference in behavior depends on several criteria such as, first and foremost, the temperature ranges of the reactions likely to release water vapor as well as the associated quantities of water.

Since a number of model parameters cannot be easily and accurately characterized, a thorough uncertainty analysis would be difficult to perform. However, parametric studies have been carried out in order to evaluate the sensitivity of the results to these parameters. In this paper, two of them are discussed, namely the porosity of the material and the condensation coefficient. It has been found that they affect the thermal evolution of the system according to threshold effects and have significant

sensitivity only in an extreme (lower) portion of their range of variation. Other model parameters (not addressed in this paper for the sake of conciseness) such as the condensation temperature (which is pressure dependent) and material related data such as the amount of released water associated to each decomposition reaction can also impact the simulation results.

From an engineering application point of view, it can be concluded that the simplified conduction-only model remains conservative with respect to the instantaneous temperature levels. It is also conservative with respect to the cumulative thermal load over time, an integral indicator that can be involved in the criteria of thermal damage evaluation. However, the conduction-only model is quite likely to lead to an underestimation of the heating kinetics of the inner shell. This set of methodologies and results **could** be used to decide whether the gas transport phenomena should be systematically taken into account in future thermal analyzes, or whether an intermediate simplified approach such as the estimation and use of apparent thermophysical parameters and heat of reaction in a conductive model (without mass transfer model) should be adopted.

Funding

This research did not receive any specific grant from funding agencies in the public, commercial, or not-for-profit sectors.

References

- Alyokhina, S., 2018. Thermal analysis of certain accident conditions of dry spent nuclear fuel storage. Nucl. Eng. Technol. 1–7. <https://doi.org/10.1016/j.net.2018.03.002>
- Alyokhina, S., Kostikov, A., 2014. Equivalent thermal conductivity of the storage basket with spent nuclear fuel of VVER-1000 reactors. Kerntechnik 79, 484–487. <https://doi.org/10.3139/124.110443>
- Bajwa, C.S., 2002. An Analysis of a Spent Fuel Transportation Cask Under Severe Fire Accident Conditions, in: Transportation, Storage, and Disposal of Radioactive Materials. ASME, pp. 1–5. <https://doi.org/10.1115/PVP2002-1606>
- Bajwa, C.S., Adkins, H.E., Cuta, J.M., 2004. Spent Fuel Transportation Cask Response to a Tunnel Fire Scenario, in: 14th International Symposium on the Packaging and Transportation of Radioactive Materials (PATRAM). Berlin, Germany. <https://doi.org/10.1115/PVP2002-1606>
- Chang, C., Tackett, J.R., 1991. Characterization of phenolic resins with thermogravimetry-mass spectrometry. Thermochim. Acta 192, 181–190. [https://doi.org/10.1016/0040-6031\(91\)87160-X](https://doi.org/10.1016/0040-6031(91)87160-X)
- Droste, B., 2007. Testing of type B packages in Germany to environments beyond regulatory test standards. Packag. Transp. Storage Secur. Radioact. Mater. 18, 73–85. <https://doi.org/10.1179/174651007X220140>
- Gendreau, F., Leoni, E., Bourgeois, S., 2012. Casks for transportation of waste materials sensitive at radiolytic and thermal decomposition. Packag. Transp. Storage Secur. Radioact. Mater. 23, 199–202. <https://doi.org/10.1179/1746510913Y.0000000018>
- Halder, A., Dhall, A., Datta, A.K., 2011. Modeling Transport in Porous Media With Phase Change: Applications to Food Processing. J. Heat Transfer 133, 031010. <https://doi.org/10.1115/1.4002463>
- IAEA, 2012. Regulations for the Safe Transport of Radioactive Material - 2012 Edition. IAEA Safety Standards Series, Vienna.
- Incropera, F.P., DeWitt, D.P., Bergman, T.L., Lavine, A.S., 2002. Fundamentals of heat and mass transfer. Wiley, New York.
- Issard, H., 2015. Radiation protection by shielding in packages for radioactive materials, in: Sorenson, K.B. (Ed.), Safe and Secure Transport and Storage of Radioactive Materials. Woodhead Publishing, Oxford, pp. 123–140. <https://doi.org/10.1016/B978-1-78242-309-6.00009-5>
- Issard, H., 2009. Development of Neutron Shielding Materials for High Burn Up Nuclear Fuel Storage Facilities, in: SMiRT 20, Helsinki, Finland.
- Lee, R., 2007. Phenolic Resin Chemistry and Proposed Mechanism for Thermal Decomposition (Jacobs Technology / NASA report).
- Lo Frano, R., Del Serra, D., Aquaro, D., 2018. Thermal tests of a CP5.2 packaging system: Prototype and experimental test description. Prog. Nucl. Energy 105, 247–253. <https://doi.org/10.1016/j.pnucene.2018.02.004>
- Lo Frano, R., Pugliese, G., Forasassi, G., 2014. Performance of a Type IP-2 Packaging System in Accident Conditions of Transport, in: HEFAT2014 10th International Conference on Heat Transfer, Fluid Mechanics and Thermodynamics. Orlando, Florida, pp. 2087–2093.
- Lo Frano, R., Pugliese, G., Forasassi, G., 2011. Thermal analysis of a spent fuel cask in different transport conditions. Energy 36, 2285–2293. <https://doi.org/10.1016/j.energy.2010.01.041>

- Mchirgui, W., 2012. Modélisation des transferts hydriques dans les milieux poreux partiellement saturés par homogénéisation périodique - Application aux matériaux cimentaires. PhD Thesis, Université La Rochelle.
- Millington, R.J., Quirk, J.P., 1961. Permeability of porous solids. *Trans. Faraday Soc.* 57, 1200. <https://doi.org/10.1039/tf9615701200>
- Mouritz, A.P., Gibson, A.G., 2007. Fire properties of polymer composite materials. Springer Science & Business Media. <https://doi.org/10.1007/978-1-4020-5356-6>
- Pugliese, G., Lo Frano, R., Forasassi, G., 2010. Spent fuel transport cask thermal evaluation under normal and accident conditions. *Nucl. Eng. Des.* 240, 1699–1706. <https://doi.org/10.1016/j.nucengdes.2010.02.033>
- Saliba, R., Quintana, F., Pimenta Mourão, R., Márquez Turiello, R., 2014. Analysis of thermal problems in development of spent fuel transport cask for research reactors. *Packag. Transp. Storage Secur. Radioact. Mater.* 25, 16–23. <https://doi.org/10.1179/1746510914Y.0000000060>
- Sanyal, D., Goyal, P., Verma, V., Chakraborty, A., 2011. A CFD analysis of thermal behaviour of transportation cask under fire test conditions. *Nucl. Eng. Des.* 241, 3178–3189. <https://doi.org/10.1016/j.nucengdes.2011.06.017>
- Xu, Y., Yang, J., Xu, C., Wang, W., Ma, Z., 2013. Thermal analysis on NAC-STC spent fuel transport cask under different transport conditions. *Nucl. Eng. Des.* 265, 682–690. <https://doi.org/10.1016/j.nucengdes.2013.07.034>

Figures

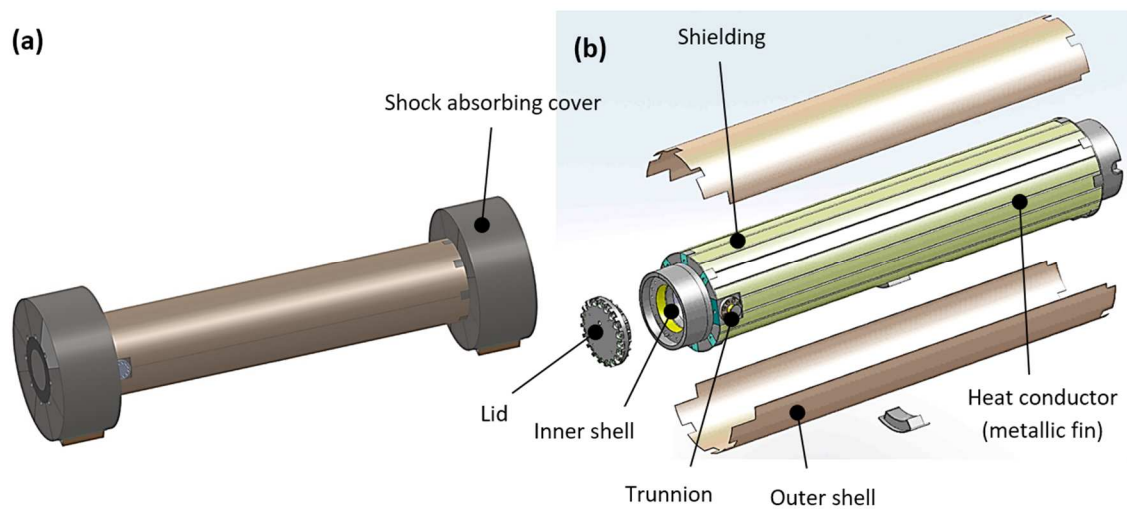


Figure 1 – Main elements of a typical transportation cask –
(a) External view – (b) Exploded view

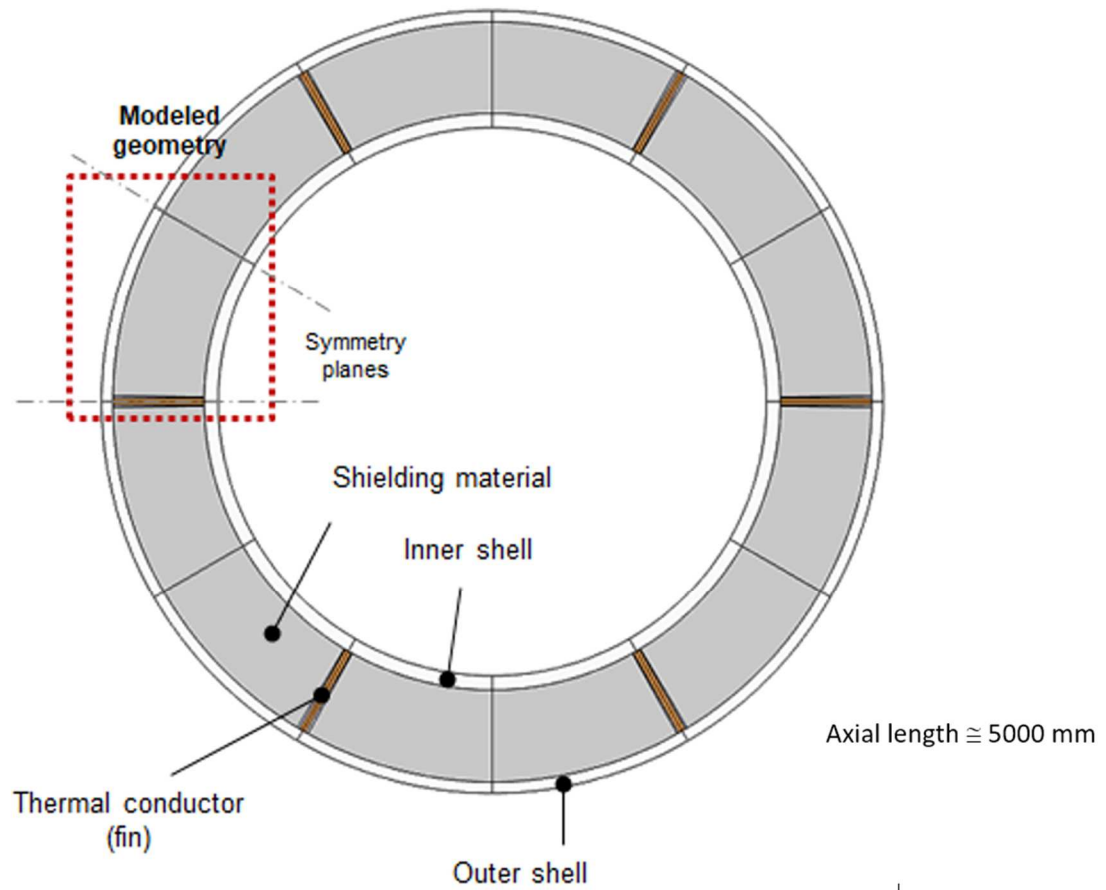


Figure 2 – Cross-section of the cask wall and modeled 2D geometry

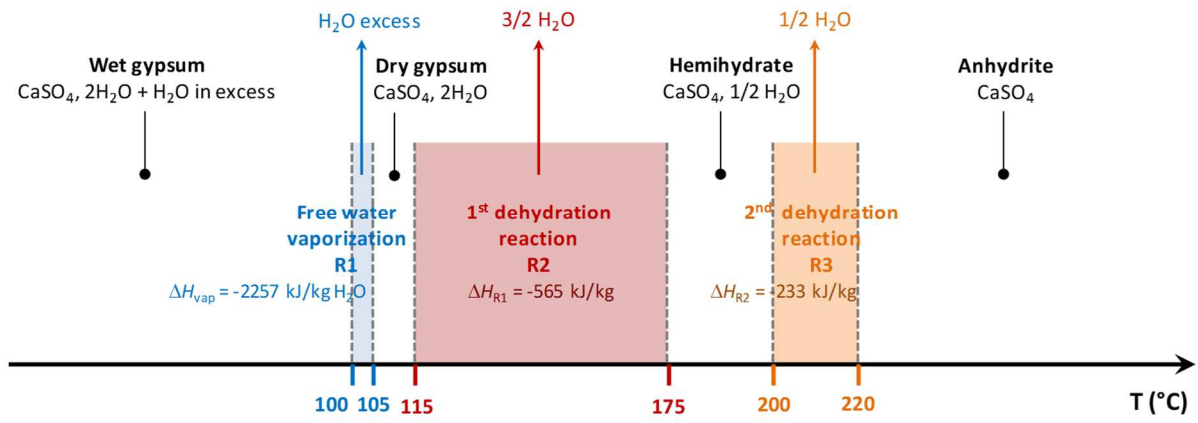


Figure 3 – Plaster dehydration reactions during heating

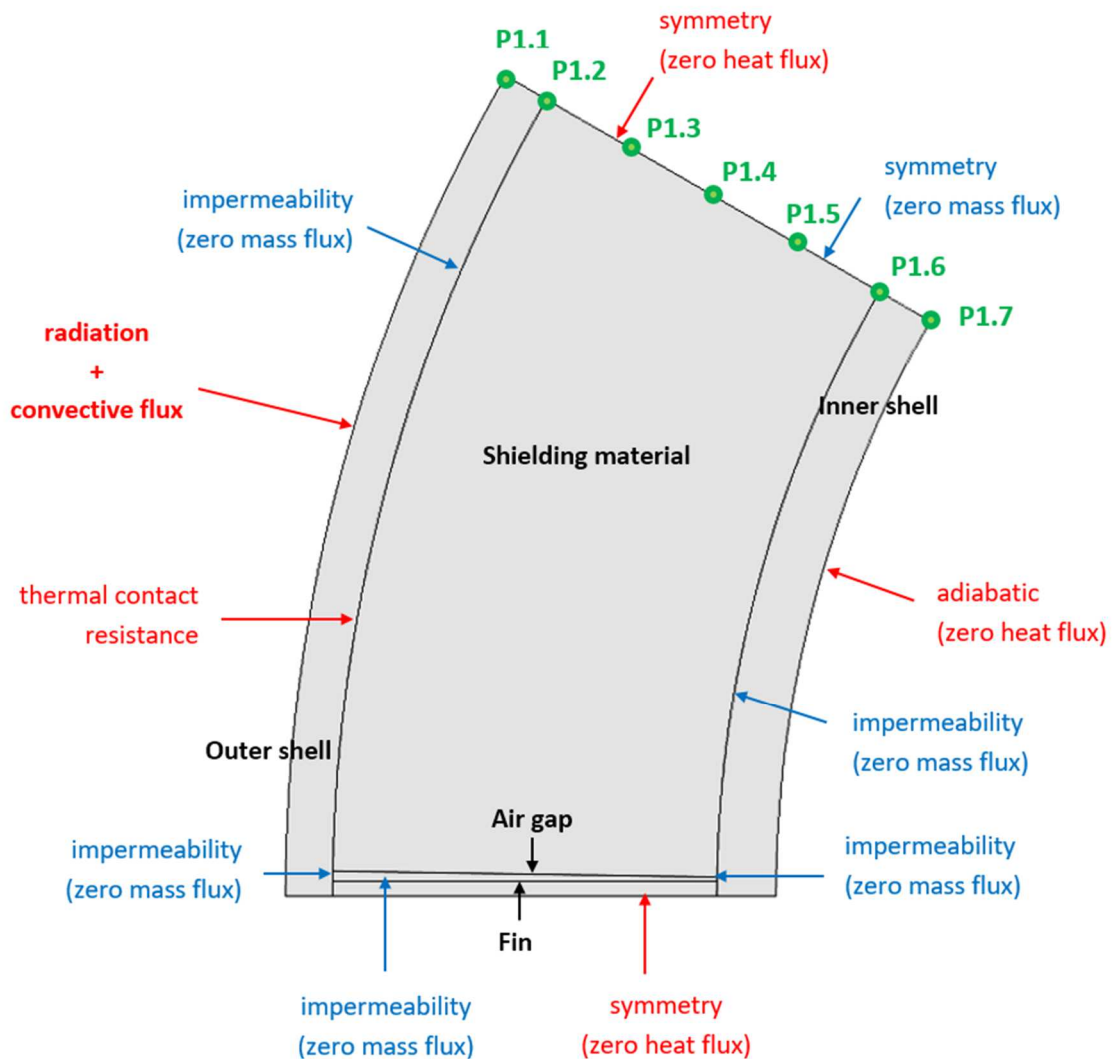


Figure 4 – Boundary conditions for heat transfer equations (red labels) and mass transfer equations (blue labels). Temperature evaluation points (green labels)

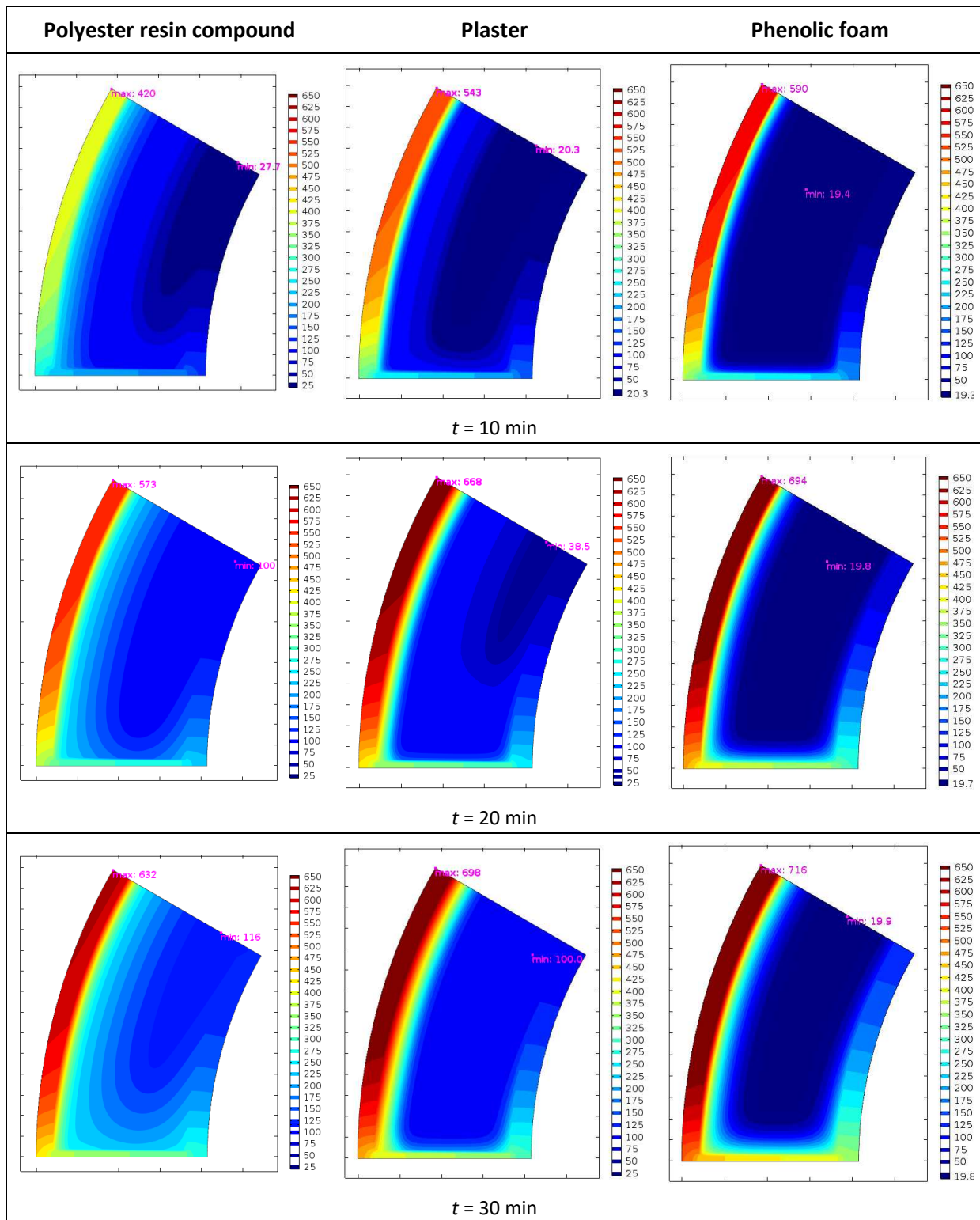


Figure 5 – Temperature field (°C) during the fire phase for PE resin compound, plaster and phenolic foam as shielding material

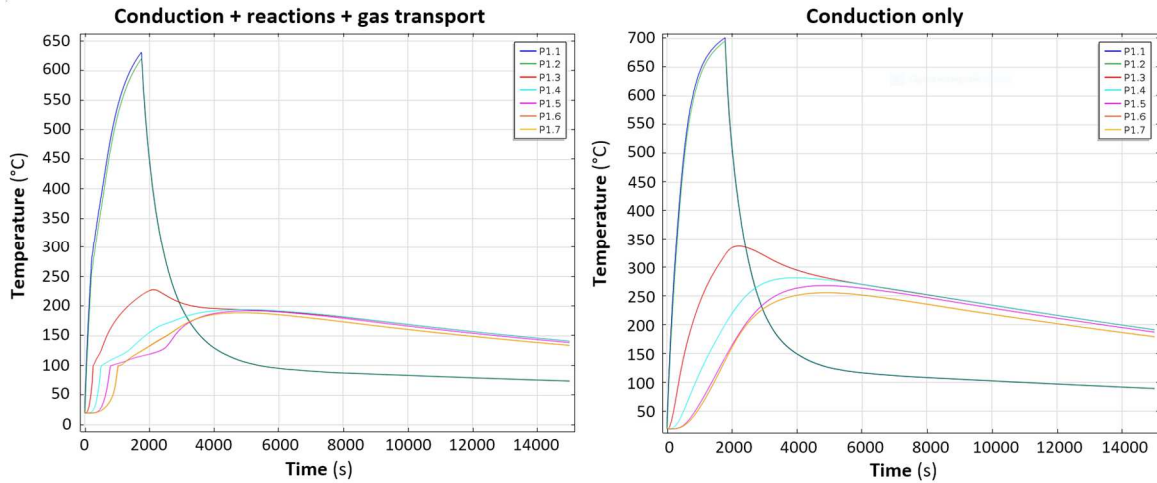


Figure 6 – Temperature evolution at several locations of the cask wall calculated with the full model and the conduction-only model - Polyester resin compound as shielding material

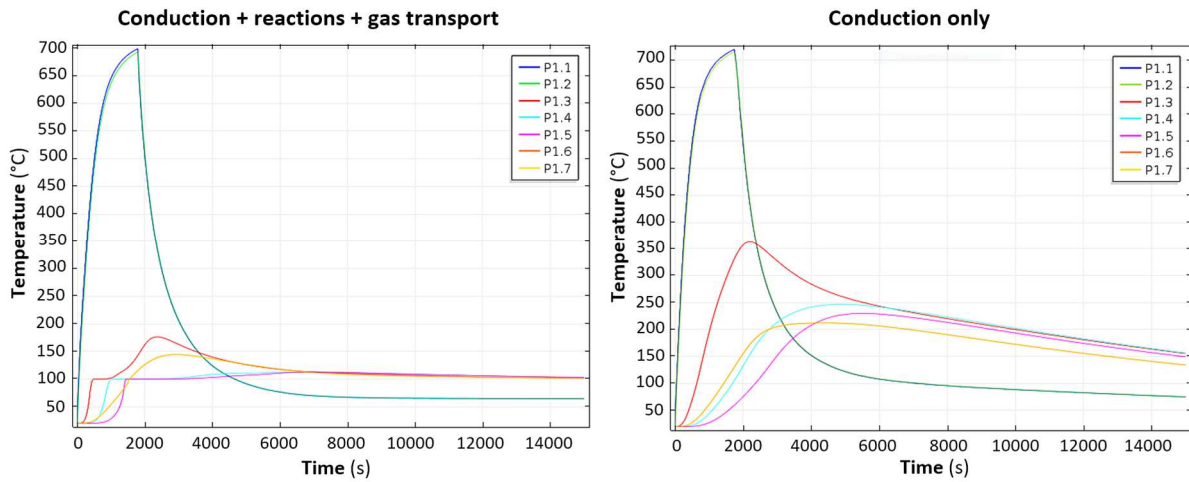


Figure 7 – Temperature evolution at several locations of the cask wall calculated with the full model and the conduction-only model - Plaster as shielding material

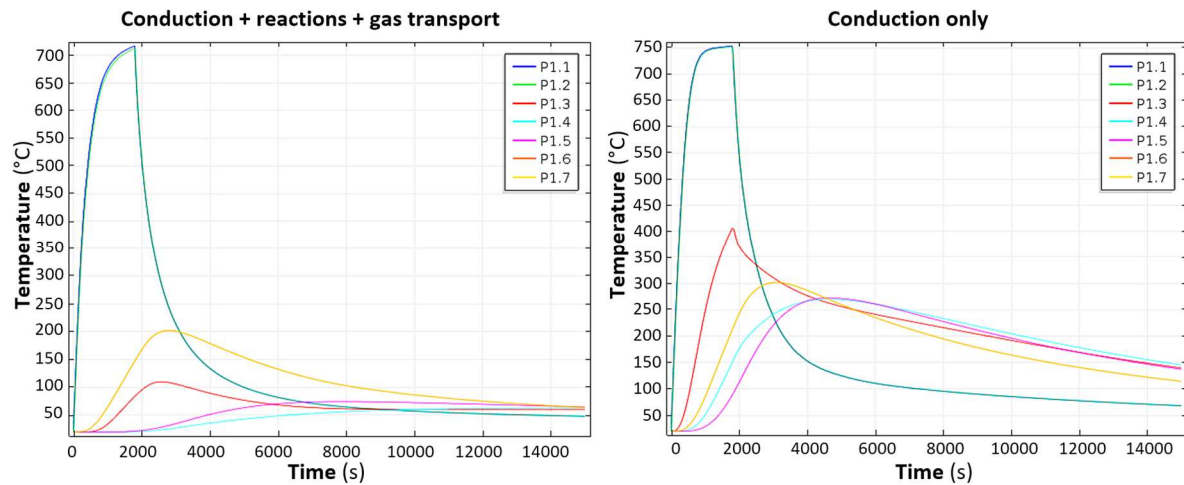


Figure 8 – Temperature evolution at several locations of the cask wall calculated with the full model and the conduction-only model – Phenolic foam as shielding material

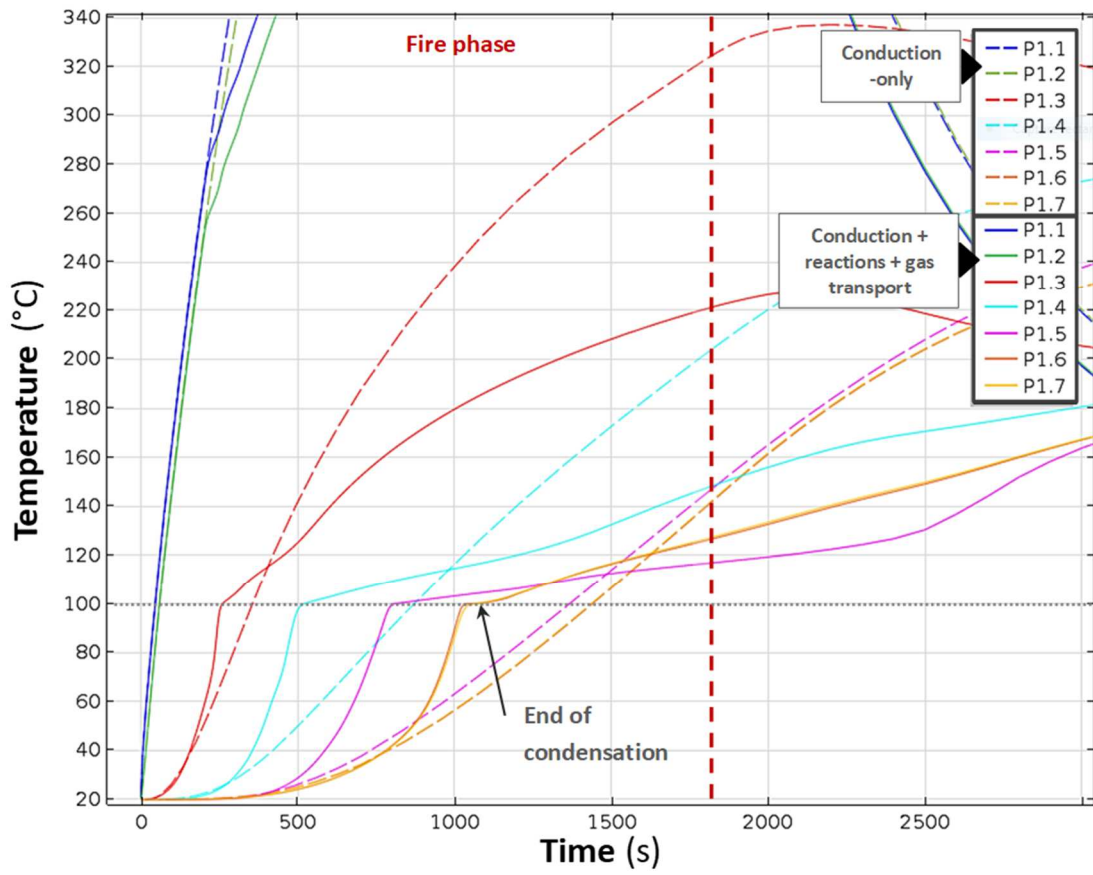


Figure 9 – Comparison of temperature evolutions calculated with the full model and the conduction-only model (polyester resin compound)

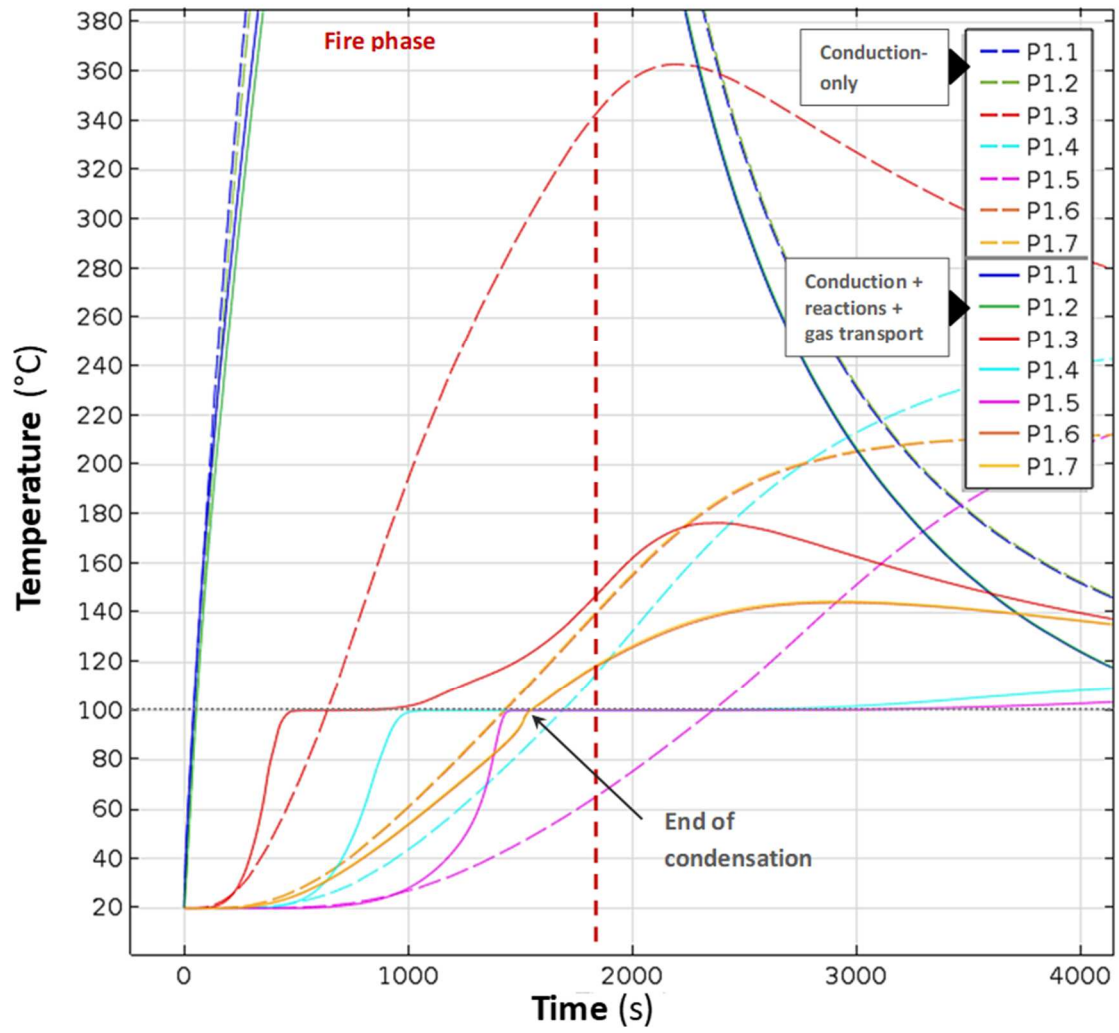


Figure 10 – Comparison of temperature evolutions calculated with the full model and the conduction-only model (Plaster)

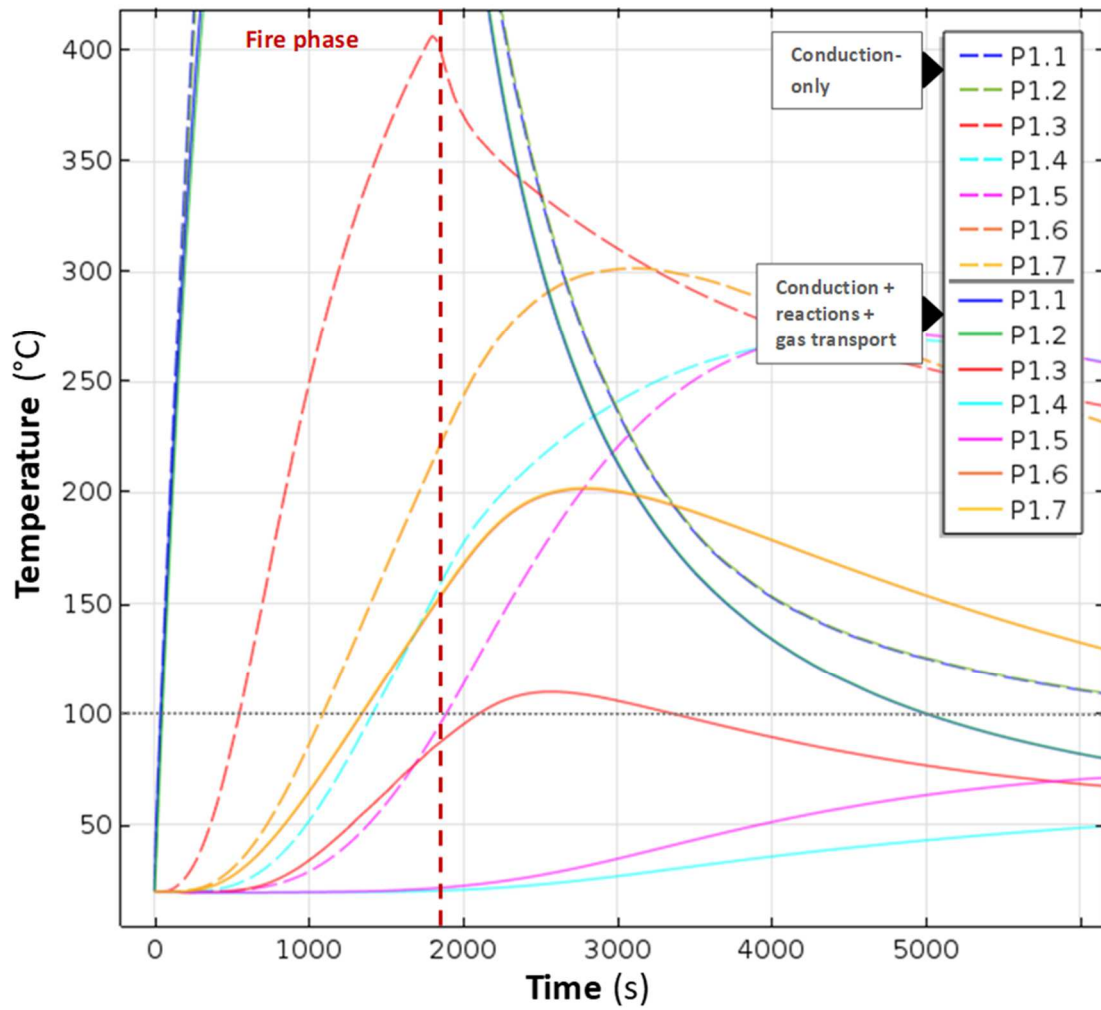


Figure 11 – Comparison of temperature evolutions calculated with the full model and the conduction-only model (Phenolic foam)

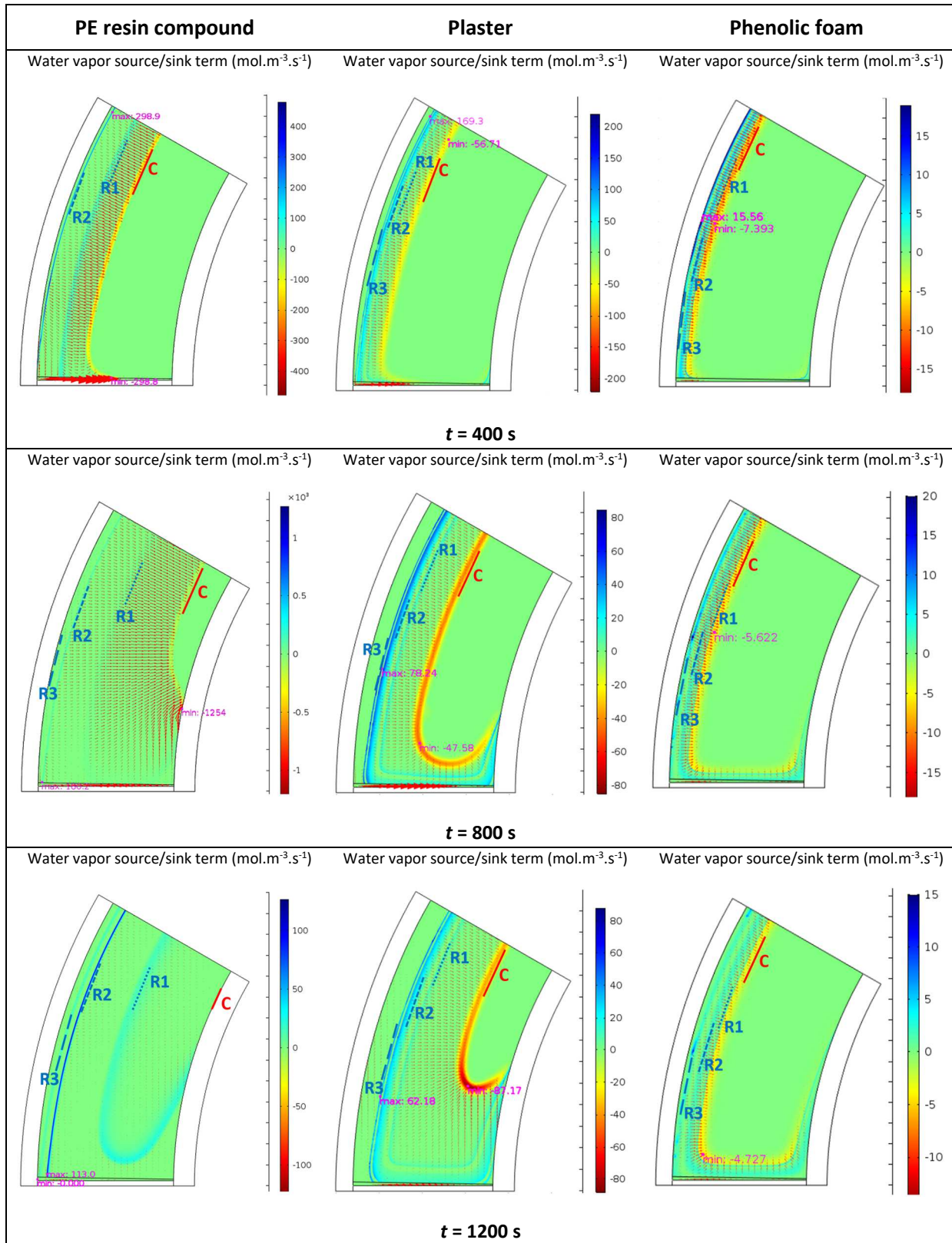


Figure 12 – Decomposition reactions fronts and water vapor transport phenomena during the fire phase for PE resin compound, plaster and phenolic foam as shielding material

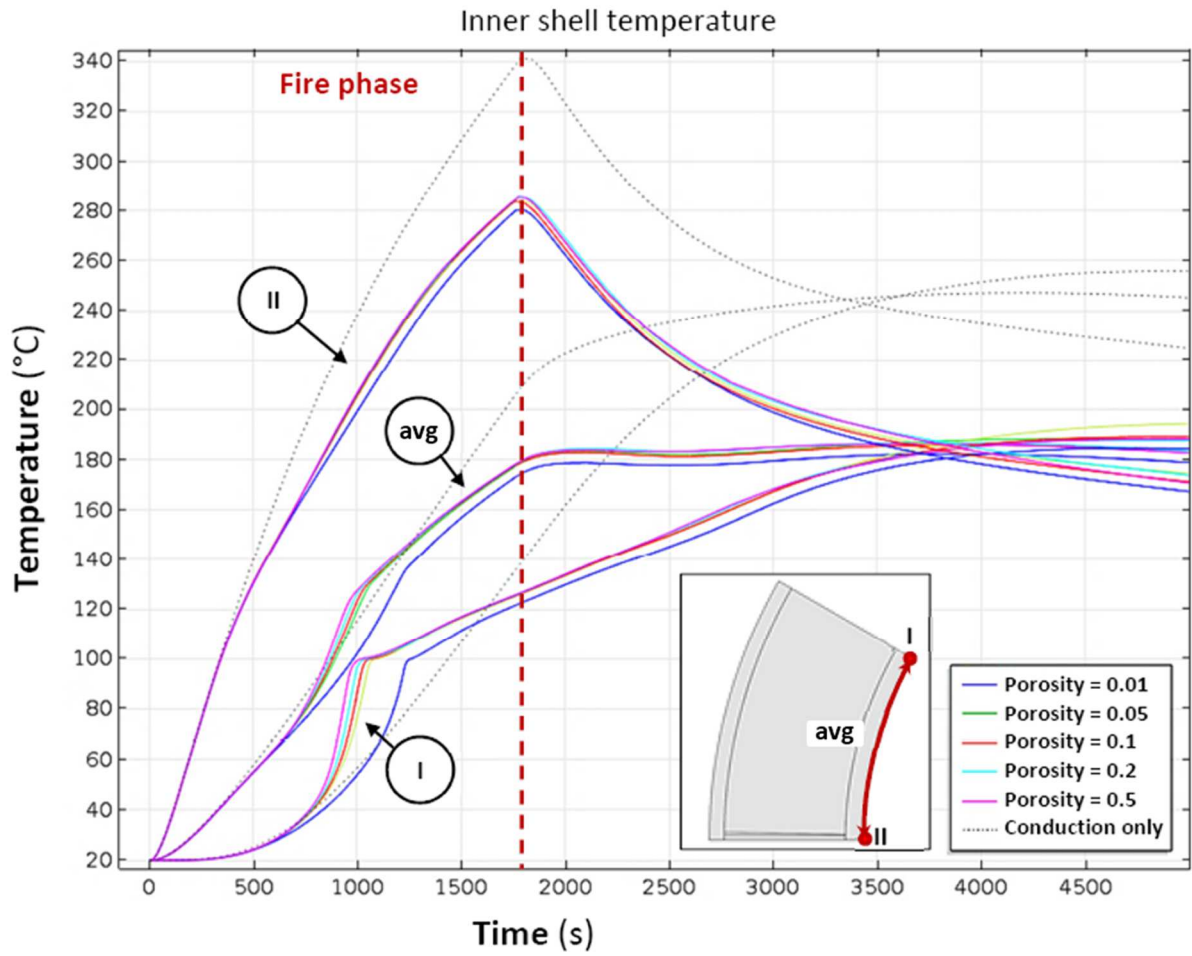


Figure 13 – Effect of the porosity parameter on the temperature evolutions of the inner shell, for polyester resin compound as shielding material

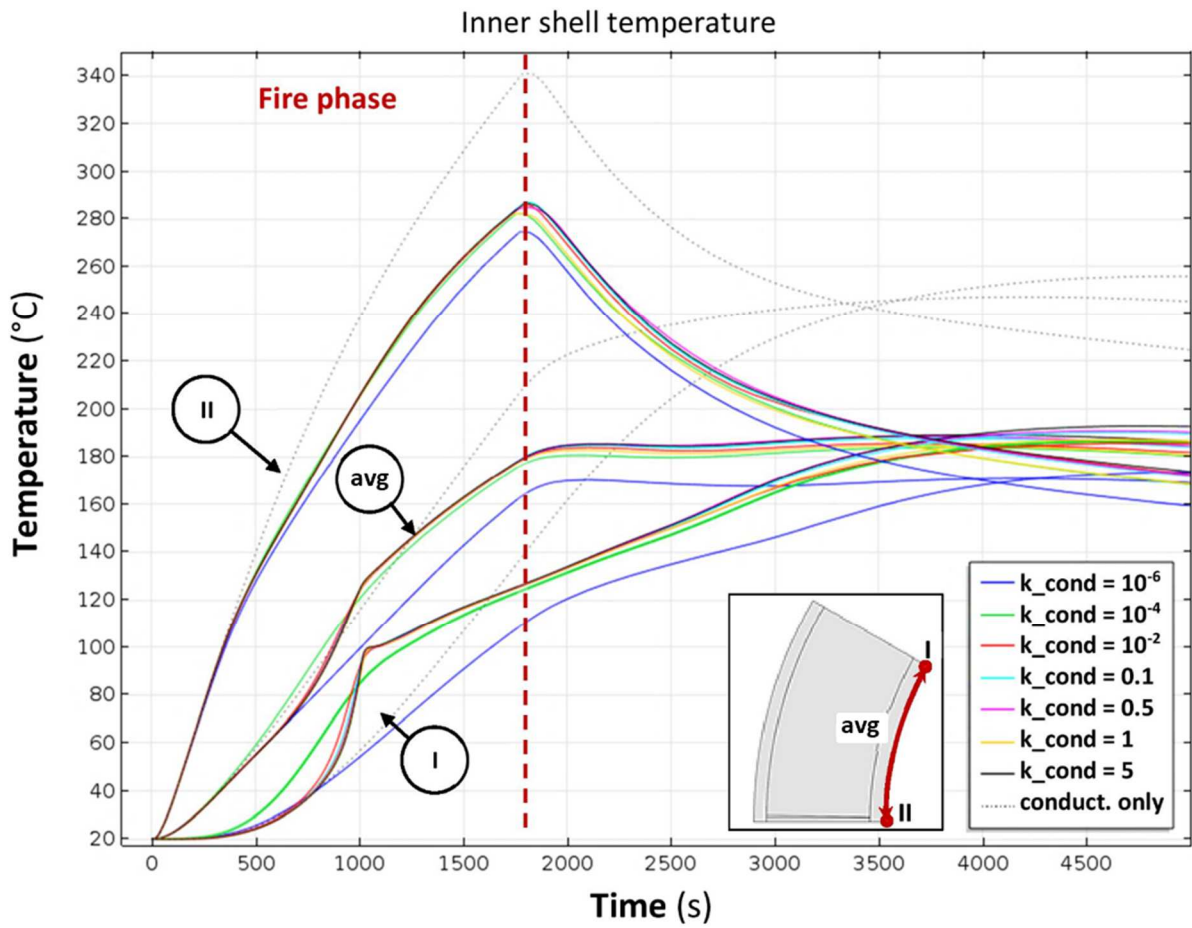


Figure 14 – Effect of the condensation coefficient parameter on the temperature evolutions of the inner shell, for polyester resin compound as shielding material

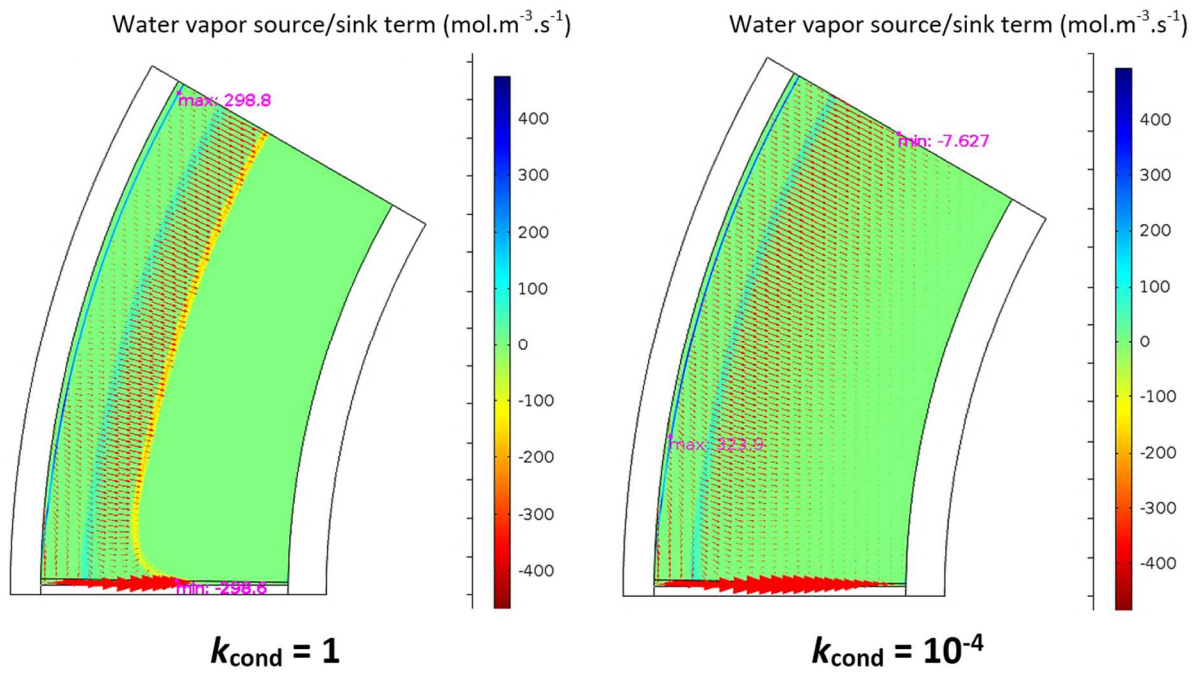


Figure 15 – Effect of the condensation coefficient parameter on the condensation zone extension (at $t = 400$ s) for PE resin compound as shielding material

Table 1 – Heat capacity and thermal conductivity of polyester resin compound

Temperature (K)	Heat capacity (J.kg ⁻¹ .K ⁻¹)	Thermal conductivity (W.m ⁻¹ .K ⁻¹)
393.15	1180	1.03
413.15	1180	1.028
443.15	1200	1.009
473.15	1280	0.956
503.15	1360	0.919
533.15	1430	0.893
553.15	1430	0.879
673.15	1430	0.4

Table 2 – Themophysical properties of the stable states of plaster

State	Density (kg.m ⁻³)	Heat capacity (J.kg ⁻¹ .K ⁻¹)	Thermal conductivity (W.m ⁻¹ .K ⁻¹)
Wet gypsum CaSO ₄ , 2 H ₂ O (+ excess water)	$2750 \frac{1.186 + \tau(G - 0.186)}{1 + 2.75G}$	$\frac{530 + 1.845 T + 4180 \tau \left(\frac{G - 0.186}{1.186} \right)}{1 + \tau \left(\frac{G - 0.186}{1.186} \right)}$	$(1 - P)k_{\text{matrix}} + \tau P k_{\text{water}} + (1 - \tau) P k_{\text{air}}$
Dry gypsum CaSO ₄ , 2 H ₂ O	$2750 \frac{1.186}{1 + 2.75G}$	$530 + 1.845 T$	$(1 - P)k_{\text{matrix}} + P k_{\text{air}}$
Hemihydrate CaSO ₄ , 1/2 H ₂ O	$2750 \frac{1}{1 + 2.75G}$	$331 + 1.757 T$	
Anhydrite CaSO ₄	$2750 \frac{0.938}{1 + 2.75G}$	$433 + T$	

Table 3 – Water vapor release during temperature rise of phenolic resin

Phase	Temperature range	Peak temperature	Mass loss (% of matrix mass)	Comments
1	90°C – 104°C	97°C	0.8%	Bound water vaporization
2	104°C – 270°C	187°C (2)	4.4%	Curing of phenolic resin
3	270°C – 600°C	435°C (3)	10.7%	Thermal degradation of phenolic resin

Table 4 – Advancement function $g(T)$ of the thermal degradation reaction of phenolic resin

Temperature (°C)	Advancement
20	0
103	0.037
270	0.1
433	0.45
444	0.98
700	1

Table 5 – Mass loss function $f_m(T)$ of the thermal degradation reaction of phenolic resin

Temperature (°C)	Relative density
20	1
103	0.96
270	0.9
433	0.55
444	0.02

Table 6 – Heat capacity of phenolic foam

Temperature (°C)	Heat capacity (J.kg ⁻¹ .K ⁻¹)
20	1396
50	1489
60	1422